© 2024. Published by The Company of Biologists Ltd | Journal of Experimental Biology (2024) 227, jeb246486. doi:10.1242/jeb.246486

RESEARCH ARTICLE

# Voltage-gated ion channels are expressed in the Malpighian tubules and anal papillae of the yellow fever mosquito (*Aedes aegypti*), and may regulate ion transport during salt and water imbalance

**Serena Farrell, Jocelyne Dates, Nancy Ramirez, Hannah Hausknecht-Buss and Dennis Kolosov***

## ABSTRACT

Vectors of infectious disease include several species of *Aedes* mosquitoes. The life cycle of *Aedes aegypti*, the yellow fever mosquito, consists of a terrestrial adult and an aquatic larval life stage. Developing in coastal waters can expose larvae to fluctuating salinity, causing salt and water imbalance, which is addressed by two prime osmoregulatory organs – the Malpighian tubules (MTs) and anal papillae (AP). Voltage-gated ion channels (VGICs) have recently been implicated in the regulation of ion transport in the osmoregulatory epithelia of insects. In the current study, we: (i) generated MT transcriptomes of freshwater-acclimated and brackish water-exposed larvae of *Ae. aegypti*, (ii) detected expression of several voltage-gated $Ca^{2+}$, $K^+$, $Na^+$ and non-ion-selective ion channels in the MTs and AP using transcriptomics, PCR and gel electrophoresis, (iii) demonstrated that mRNA abundance of many altered significantly following brackish water exposure, and (iv) immunolocalized $Ca_V1$, NALCN, TRP/Painless and KCNH8 in the MTs and AP of larvae using custom-made antibodies. We found $Ca_V1$ to be expressed in the apical membrane of MTs of both larvae and adults, and its inhibition to alter membrane potentials of this osmoregulatory epithelium. Our data demonstrate that multiple VGICs are expressed in osmoregulatory epithelia of *Ae. aegypti* and may play an important role in the autonomous regulation of ion transport.

**KEY WORDS: Insect osmoregulation, Vectors of infectious disease, Mosquito larvae, Epithelia, Voltage-gated ion channels**

## INTRODUCTION

Mosquitoes are economically important vectors of infectious diseases (e.g. malaria, Zika virus and Ebola), contributing to the annual death toll of ∼700,000 people from, and ∼4 billion people at risk of contracting, mosquito-borne infectious diseases worldwide (Lozano et al., 2012; WHO, 2014). Disease transmission occurs when the female mosquitoes take blood from humans to gain protein needed to produce eggs, and, in the process, transmit infectious disease pathogens to the human host. Following blood feeding, the female mosquito lays eggs in water, which can introduce vectors of infectious diseases into new areas not yet affected by an established mosquito population. Recent incursions into regions that do not usually have permanent breeding populations create a direct threat (Scheffers et al., 2016).

The mosquito life cycle consists of a filter-feeding aquatic larval life stage hatching from eggs laid in water, after which developing larvae pupate and metamorphose into terrestrial adults. Mosquito larvae can be found in diverse aquatic habitats and, in general, demonstrate an extensive range of salinity tolerance compared with most animals (Bradley, 1994). Most *Ae. aegypti* larvae develop in a constant salinity (mostly freshwater, FW), larvae of females that do choose to lay eggs in brackish water (BW) near coastline may experience fluctuations in salinity, with documented cases ranging from 2 to 18 ppt (Ramasamy et al., 2011), and established survival in up to 10 ppt (e.g. de Brito Arduino et al., 2015). These larvae are often faced with rapid changes in salinity caused by heavy rainfall, evaporation, or incursion of seawater (Bradley, 1987). Worldwide, *Ae. aegypti* are increasingly present in BW habitats and more northern latitudes, currently reaching as far as Canada in North America, with projections predicting expanding habitat range worldwide (Ramasamy et al., 2011, 2014; Surendran et al., 2012; Lounibos and Kramer, 2016; Ramasamy and Surendran, 2016; Surendran et al., 2018a,b; Parker et al., 2019; Giordano et al., 2020; Khan et al., 2020; Brennan et al., 2021). This includes Southern California, where *Ae. aegypti* has established breeding populations across the state counties stemming from recent introduction from multiple genetically divergent source populations – it has recently been detected in 72% of households in Los Angeles County, posing increased risk of infectious disease transmission and spread for inhabitants of coastal cities that surround ocean and brackish waters (Lee et al., 2019; Donnelly et al., 2020). Southern California lacks natural FW habitats and mosquito eggs are typically laid by blood-fed females into bodies of standing water created by human activity or in bodies of FW, which often connect with the ocean. Thus, all larvae hatched from eggs laid in FW actively hyper-osmoregulate, keeping hemolymph ion concentrations higher than those of FW. However, larvae may end up drifting downstream towards the ocean through BW. Eggs laid in small human-made standing bodies of water can face rapid evaporative water loss, increasing in salinity and nitrogenous waste content as larvae develop (Bradley, 1987). In fact, the recent spread of *Ae. aegypti* may be due to its ability to tolerate saline BW that surrounds coastal cities, where the capacity of some populations to complete their life cycle in BW is considered a heritable trait (Lee et al., 2019).

The Malpighian tubules (MTs) are an osmoregulatory organ found in both adult and larval mosquitoes, consisting of a multifunctional epithelium, which together with the hindgut is essential for the maintenance of solute and water homeostasis,

Department of Biological Sciences, California State University San Marcos, 333 S. Twin Oaks Valley Road, San Marcos, CA 92096, USA.

*Author for correspondence (dkolosov@csusm.edu)

D.K., 0000-0003-3581-9991

**Received 28 July 2023; Accepted 22 December 2023**

Journal of Experimental Biology (2024) 227, jeb246486. doi:10.1242/jeb.246486

acid–base balance and nitrogenous waste excretion, among other functions (Piermarini and Gillen, 2015; Esquivel et al., 2016; Piermarini et al., 2017a). MTs of FW-dwelling larvae produce isosmotic urine, which is modified by the rectum via KCl reabsorption to conserve ions (recycling ions between MTs and the rectum to move excess water out via the urine). In contrast, post-prandial urine production by MTs in blood-fed females is plentiful, but urine is closer to being isosmotic, containing both ions and water from a recent blood meal (Bradley, 1994; Drake et al., 2010; Li et al., 2017). Ion transport is achieved via principal and secondary epithelial cells of the MTs, which carry out cation and anion transport, and thus directly enable the excretory function of the MTs by creating an osmotic gradient that draws water into the tubule (Beyenbach and Piermarini, 2011). Mechanisms of ion transport in the MTs of mosquitoes are well studied, whereas the regulation of ion transport remains largely understudied.

The anal papillae (AP) are exclusively larval osmoregulatory organs that are in direct contact with the external aquatic environment. Classical ultrastructural and functional studies revealed that these sac-like structures are filled with hemolymph and are syncytial in nature (Koch, 1938; Treherne, 1954; Ramsay, 1953; Sohal and Copeland, 1966). In FW habitats, AP actively sequester ions and experience diffusional water uptake from surrounding FW (Wigglesworth, 1933; Marusalin et al., 2012), and are capable of completely replenishing $Na^+$ and $Cl^-$ content of the hemolymph in ∼3 h (Donini and O'Donnell, 2005; Durant et al., 2021). The larvae are known to survive in more saline habitats, with AP altering in ultrastructure, ion and water transport kinetics, and gene expression, but remaining functional despite fluctuating salinities over the course of larval development (Stobbart, 1971; Donini et al., 2007; Marusalin et al., 2012; Akhter et al., 2017; Surendran et al., 2018a,b; Durant et al., 2021). Molecular mechanisms of ion transport in AP of mosquitoes have recently been described; however, the detailed mechanisms of its regulation remain to be studied (Donini and O'Donnell, 2005; Patrick et al., 2006; Del Duca et al., 2011; Durant et al., 2021).

Larvae of *Ae. aegypti* maintain salt and water balance during BW exposure using a combination of the hindgut, the MTs and AP, resulting in hemolymph osmolality equivalent to BW, but without active osmoconformation (Bradley, 1994). Multiple studies report that *Ae. aegypti* can be reared in, or abruptly exposed to, ∼30% seawater, although detailed mechanisms of how short-term variations in environmental salinity are detected and handled by the osmoregulatory tissues of mosquito larvae remain unclear (e.g. Edwards, 1982; Donini et al., 2006, 2007; Jonusaite et al., 2016, 2017; Durant et al., 2021). Recent transcriptomic surveys revealed that voltage-gated ion channels (VGICs) are expressed in all non-innervated non-contractile osmoregulatory epithelia of animals studied to date (Kapoor et al., 2021; Durant et al., 2021; Kolosov and O'Donnell, 2022). VGICs are often ion selective and can respond rapidly to changes in membrane potential ($V_m$) (Kariev and Green, 2012). In insect MTs, specifically, voltage-gated $Ca_V1$ and HCN channels have recently been shown to directly regulate ion transport in the MTs of larval lepidopterans (Kolosov and O'Donnell, 2019; Kolosov et al., 2021).

In mosquitoes, MTs and AP are simple epithelial organs with tracheae – neither is innervated or capable of peristaltic movement; thus, all regulation of MT ion transport must be endo/auto/paracrine, or aided by autonomous osmosensing of the organ (Edwards and Harrison, 1983; Coast, 1998). Additionally, lack of innervation or muscle layers eliminates the confounding variables of VGIC contribution to the regulation of ion transport via neuronal/muscular pathways. The objectives of the current study were to: (i) generate MT transcriptomes of FW-acclimated and BW-exposed larvae of *Ae. aegypti*, (ii) detect all VGICs expressed in the MTs and AP, (iii) investigate whether VGICs alter in mRNA abundance in MTs and AP of larvae exposed to BW, and (iv) investigate whether select VGIC proteins are expressed in these osmoregulatory epithelia. We demonstrate that multiple VGICs are expressed in MTs and AP epithelia of larval *Ae. aegypti*, and that the abundance of several changes with BW exposure. As $Ca_V1$ has been shown by our recent study to be involved in the regulation of ion transport in the MTs of larval lepidopterans (Kolosov et al., 2021), we additionally show that $Ca_V1$ may be specifically linked to ion transport in the MTs of *Ae. aegypti*.

## MATERIALS AND METHODS

### Experimental animals and salinity exposure

Eggs of *Aedes aegypti* (Linnaeus) were obtained from Benzon Research (Carlisle, PA, USA), which provided the basis for the lab *Aedes* colony. Eggs were hatched in dechlorinated FW ([$Na^+$] 19.2±5.6 µmol $l^{-1}$, [$Cl^-$] 44.3±15.5 µmol $l^{-1}$). Larvae were fed a diet of inactivated yeast and liver powder, water was replaced every 2 days and larval density was maintained throughout development at 50 larvae $l^{-1}$. Pupae were transferred to bug dorms daily, where adult *Ae. aegypti* were kept and fed 5% aqueous sucrose solution and warmed-up Alsevers sheep blood (Carolina Biological Supply Company, Burlington, NC, USA). Lab temperature is maintained at 21°C throughout the year, and the light:dark cycle is maintained at 12 h:12 h using timed light fixtures.

For salinity exposure experiments, several groups of 100 larvae were exposed to different salinities. Half the containers were exposed to a typical water change to FW. The other half were exposed to 10 ppt BW ([$Na^+$] 132.0±4.2 mmol $l^{-1}$, [$Cl^-$] 151.9 ±3.1 mmol $l^{-1}$) for 24 h. Salinity exposure containers were set up in a paired and staggered manner to allow for prompt dissection of tissues of larvae exposed to salinities for ∼24 h. BW was made in the lab using Instant Ocean aquarium salt (United Pet Group Inc., Cincinnati, OH, USA) and double-distilled water. This mixture was measured using a portable refractometer until 10 ppt was reached.

### Hemolymph collection and ion-selective microelectrode analysis

Hemolymph was collected from BW- and FW-exposed larvae under hydrated oil by gently puncturing the exoskeleton with iris microscissors. Larvae were captured and briefly rinsed in double-distilled water to wash environmental salt off the exoskeleton. Collected hemolymph samples were immediately analyzed for ion content using ion-selective microelectrodes constructed according to Donini and O'Donnell (2005). Briefly, $K^+$- and $Na^+$-selective microelectrodes were constructed by pulling glass microcapillaries (cat. no. B150-110-10, Sutter Instruments, Novato, CA, USA) on a PUL-1000 microelectrode puller (World Precision Instruments, Inc., Sarasota, FL, USA) with a barrel diameter of ∼2–3 µm. Freshly pulled microelectrodes were silanized and baked, and kept in a desiccator until further use. $K^+$ Ionophore 1–cocktail A was purchased (cat. no. 99311, Sigma-Aldrich, St Louis, MO, USA). $Na^+$ ionophore was prepared in the lab, and consisted of (w/w): 3.5% $Na^+$ ionophore X (cat. no. 71747, Sigma-Aldrich), 0.6% potassium tetrakis(4-chlorophenyl)borate (cat. no. 60591, Sigma-Aldrich) and 95.9% 2-nitrophenyl octyl ether (cat. no. 73732, Sigma-Aldrich). On the day of use, ion-selective electrodes were constructed by back-filling the glass microelectrode with 150 mmol $l^{-1}$ KCl or NaCl, front-filling it with the liquid-state

ionophore cocktails mentioned above, and calibrating in the following solutions: $K^+$, 1.5 mmol $l^{-1}$ and 15 mmol $l^{-1}$; $Na^+$, 15 mmol $l^{-1}$ and 150 mmol $l^{-1}$. Solid-state Cl- electrodes were constructed according to Kolosov and O'Donnell (2020), and calibrated in 15 and 150 mmol $l^{-1}$ NaCl. All calibration solutions were balanced to maintain constant ionic strength. Ion-selective microelectrodes and reference electrodes (non-silanized, back-filled with 150 mmol $l^{-1}$ KCl) were connected to a high-impedance electrometer (ML165 pH Amp, ADInstruments, Colorado Springs, CO, USA), which in turn was connected to a PowerLab 2/26 data acquisition system running LabChart software (ADInstruments, Sydney, NSW, Australia). Hemolymph ion concentration measurements were conducted under oil and ion-selective microelectrode data were acquired and analyzed using LabChart software. Voltage readings from hemolymph samples were used to back-calculate ion concentrations in the samples using the following equation: $[\text{ion}]_{\text{sample}}=[\text{ion}]_{\text{standard}}\times 10^{(dV/S)}$, where $[\text{ion}]_{\text{sample}}$ is hemolymph ion concentration, $[\text{ion}]_{\text{standard}}$ is ion concentration in the calibration solution, $dV$ is the difference in voltage between the hemolymph and the calibration solution, and $S$ is the Nernstian slope of the electrode measured in response to a 10-fold change in ion concentration.

### Microdissections and tissue sampling: MTs and AP

Microdissections of larval *Ae. aegypti* were performed under a stereomicroscope in larval saline containing (in mmol $l^{-1}$) 30 NaCl, 25 Hepes, 3 KCl, 5 $NaHCO_3$, 0.6 $MgSO_4$, 5 $CaCl_2$, 5 glucose, 5 proline, 9.1 glutamine, 8.74 histidine, 14.4 leucine, 3.37 arginine, 5 succinic acid, 5 malic acid and 10 tri-sodium citrate, pH 7.10 (Donini et al., 2007) (all chemicals were purchased from fisher scientific, ThermoFisher Scientific, Carlsbad, CA, USA). Larvae were pinned down by the head and MTs and AP were dissected out in larval *Aedes* saline. Tissue samples were manipulated and microdissected out using Dumont 5 ultrafine forceps and glass microprobes custom-made in the lab, while carefully and diligently removing tracheal connections and surrounding tissues to ensure no other tissues were harvested together with AP or MTs. The tissue samples were stored in Eppendorf tubes filled with 500 µl of RNAlater® Stabilization solution (ThermoFisher Scientific) and samples were collected for each osmoregulatory tissue in each salinity type. Each biological replicate contained 200 MTs or 160 AP microdissected out of 40 larvae from the same treatment group. During collection time, previously harvested biological replicates were stored at 4°C. Tissue collection was always performed in a timed and paired manner to ensure ∼24 h of salinity exposure and the side-by-side collection of the two salinity treatment samples.

### RNA extraction and purification, and cDNA synthesis

RNA extraction (RNA precipitation, wash and redissolving) was performed using TRIzol reagent (ThermoFisher Scientific) according to the manufacturer's instructions as described in Kolosov et al. (2019). Briefly, larvae were dissected in larval *Aedes* saline and tissues collected as described above. Following microdissection and storage in RNAlater®, tissues were homogenized in Trizol® using a 26G syringe needle and total RNA was extracted following the manufacturer's protocol. RNAlater was removed by aspiration and tissues were immersed in 0.5 ml Trizol (ThermoFisher Scientific) per biological replicate. Tissues were homogenized in Trizol using a 26G syringe needle and allowed to remain at room temperature for 5 min to dissociate nucleoprotein complexes. Molecular grade chloroform (100 µl) was then added to every sample. Tubes were vigorously agitated by hand and incubated at room temperature for 3 min. Samples were then centrifuged at 12,000 ***g*** for 15 min at 4°C to perform phase separation, after which the clear aqueous phase containing total RNA was collected into a set of new, sterile 1.5 ml Eppendorf tubes and kept on ice. Molecular grade isopropanol (250 µl) was added to every sample to precipitate RNA. Tubes were agitated gently and left at room temperature for 10 min, after which they were centrifuged at 12,000 ***g*** for 10 min at 4°C to concentrate the precipitate into the pellet. Supernatant was removed from every tube by aspiration and pellets were washed in 75% molecular grade ethanol solution in RNase-free water, and centrifuged at 7500 ***g*** for 5 min to immobilize pellets. Ethanol was then removed by aspiration and pellets were left to air-dry for 1 min at room temperature, after which they were dissolved in 12 µl of RNase-free water. Total RNA was purified using a Thermo Scientific GeneJet RNA Cleanup and Concentration Micro Kit (cat. no. K0841, ThermoFisher Scientific). The concentration and quality of purified RNA were determined using a nano-sample spectrophotometer (DeNovix DS-11, Wilmington, DE, USA). Absorbance ratios of $A_{260}/A_{280}$=2.11±0.01 and $A_{260}/A_{230}$=2.08±0.03 were observed, indicating excellent purity of samples free of contamination. Total purified RNA from 3 biological replicates for each salinity treatment group was sent to University of California Riverside Genomics Facility for Illumina library preparation (see 'RNAseq library preparation, sequencing, quality control, mapping and differential expression analysis', below).

Following a similar RNA extraction and purification process, 2 µg of total RNA, treated with DNAse, was used for oligo-dT-aided reverse-transcriptase cDNA synthesis. cDNA was diluted in RNAse/DNAse-free water and used for PCR and qPCR (see 'PCR/qPCR amplification and gel electrophoresis', below).

### RNAseq library preparation, sequencing, quality control, mapping and differential expression analysis

Single-end 75 bp Illumina libraries were prepared by the University of California Riverside Institute for Integrative Genome Biology sequencing facility (UCR IIGB, Riverside, CA, USA) using the following methodology. Total RNA samples were screened with an Agilent Bioanalyzer 2100 to confirm quality and concentration. Each sample was diluted to 250 ng for input into NEBNext Poly(A) mRNA Magnetic Isolation Module (E4790, New England Biolabs), followed by NEBNext Ultra II Directional RNA Library Prep kit for Illumina (E7760). The NEB protocol was followed with the following adjustments: 0.8× bead clean after second strand synthesis, adaptor dilution of 1:30, 0.7× bead clean after ligation, 15 cycles of amplification, and dual bead clean after enrichment. Standard Illumina adaptors were used for all, but each library was barcoded independently with TruSeq indexes. Final libraries were qualified and quantified with Agilent Bioanalyzer 2100, then pooled equimolarly. Sequencing was performed with Illumina NextSeq500 using a High-output Single-end 75 bp kit.

Sequencing (at UCR IIGB) of six strand-specific libraries (3 FW exposed and 3 BW exposed) with 75 bp single-end reads yielded a total of 398,425,646 reads with an average of ∼66.4 million of raw reads per library. Quality control (QC) reports were performed by UCR IIGB and 100% of reads with a read length of exactly 75 bp were subjected to quality control trimming with Trimmomatic using previously described protocols (usegalaxy.org; Goecks et al., 2010; Kolosov et al., 2019). Raw sequencing data are available at SRA BioProject (PRJNA1068135).

The AaegL5.0 *A. aegypti* transcriptome was accessed at ncbi.nlm.nih.gov and official genome transcript annotation was used for

mapping. Mapping of Next Generation Sequencing (NGS) reads to this transcript set was performed using Salmon (Galaxy version 1.3.0, usegalaxy.org) mapping software (Patro et al., 2017). Mapping was performed to the *Ae. aegypti* transcriptome and annotation supplied with the official genome annotation was used.

Differential expression analysis was performed in R (version 3.4.2) using the DESeq2 package (release 3.7) (Love et al., 2014), where the BW-exposed group was compared with the FW-exposed group. This analysis involved compiling counts tables for all samples generated by Salmon in Galaxy, uploading them to R, creating a metadata table indicating which sample belongs to which treatment group, and running the DESeq2 script in R as instructed in the vignette publication, which estimates size factors and dispersions, determines mean dispersion relationship, and builds a model of differential expression. DESeq2 analysis in R resulted in a list of all differentially expressed transcripts (Table S1) accompanied by the $\log_2$ fold-change ($\log_2$FC), *P*-value of the change (*P*) and *P*-value adjusted ($P_{adj}$) for the false discovery rate (FDR) by the DESeq2 Benjamini–Hochberg algorithm. For further information, the reader is directed to Love et al. (2014).

### PCR/qPCR amplification and gel electrophoresis

Detailed analysis of NGS data suggested that multiple voltage-gated, ligand-gated and mechanosensitive ion channels (VGICs, LGICs and MSICs, respectively) were expressed in the MTs of larval *Ae. aegypti*. Expression of transcripts encoding VGICs was determined by RT-PCR in MTs and AP using Platinum or DreamTaq Hot-Start Supermix (ThermoFisher Scientific). Changes in transcript abundance in MTs and AP of BW-exposed larvae were assessed using quantitative real-time PCR (qPCR) with 2× DyNAmo Flash SYBR Green qPCR Mastermix (F415L, ThermoFisher Scientific), a BioRad PCR machine for RT-PCR (PTC-2000; Bio-Rad Laboratories Canada Ltd, Mississauga, ON, Canada) and ThermoFisher Scientific QuantStudio 3 qPCR machine running ABM Design and Analysis software. Primers specific for VGICs were designed based on sequences obtained from RNAseq experiments. Gel electrophoresis was performed on PCR amplicons to confirm their size, and electrophoresed samples were subsequently extracted from the gel, purified and sequenced to ensure that amplicon identity was in line with designed parameters, and submitted to GenBank for annotation (see Table 1 for PCR primer and cycling information).

The following reaction conditions were used: 1 cycle for denaturation (95°C, 4 min), followed by 40 cycles of: denaturation (95°C, 30 s), annealing (see Table 1, 30 s) and extension (72°C, 30 s), with a final extension step (72°C, 10 min). To ensure that a single PCR product was synthesized during reactions, a dissociation curve analysis was carried out after each qPCR run. Transcript abundance was normalized to that of *Ae. aegypti* actin (*act*). The use of *act* for gene of interest normalization in salinity exposure studies was validated by statistically comparing tub threshold cycle values between tissues to confirm that no statistically significant changes occurred ($P$=0.842 for MTs and $P$=0.4688 for AP, Student's *t*-test).

### Immunohistochemistry: whole-mount and cross-sections

Whole-mount immunohistochemistry (IHC) procedures have been described in detail elsewhere (Kolosov et al., 2018a; Patrick et al., 2006). Briefly, larvae were dissected in larval saline (as described above); adult tissues were dissected in adult saline (in mmol $l^{-1}$: 150 NaCl, 3.4 KCl, 1.8 $NaHCO_3$, 1.7 $CaCl_2$, 1.0 $MgSO_4$, 25 Hepes and 5.0 glucose; Yu and Beyenbach, 2002). After dissection in appropriate saline, MTs or AP were removed and fixed in 4% paraformaldehyde (PFA) in phosphate-buffered saline (PBS, pH 7.4) overnight at 4°C. The following day, tissues were washed in PBS and dehydrated (20% v/v, stepwise to 100%) and rehydrated (100% to PBS) in a methanol/PBS series. Tissues were then permeabilized and blocked in PBS containing 0.1% Triton X-100 solution (PBT), containing 2% w/v bovine serum albumin (BSA). After blocking, tissues were incubated with primary antibody overnight at 4°C at 1:100 dilution. The anti-VGIC antibodies were custom-ordered from GenScript (Piscataway, NJ, USA), epitope-affinity purified and directed against the C-terminal region of the following *Ae. aegypti* proteins encoded by mRNA detected by RNAseq and PCR (NCBI accession no.; epitope): $Ca_V1$ alpha-1 isoform (XP_021699870.1; CWSEYDPDAKGRIKH), $Na^+$ leak channel Nalcn (XP_021710075.1; MKMLGRKQSLKGEPC), voltage-gated $K^+$ channel KCNH8 (XP_021699750.1; ILKEFPEE LRGDIS) and transient receptor potential TRP/Painless (XP_001652261.2; CLTANDKRPGDDDY). An additional preparation was included with each IHC analysis, where primary antibody was omitted to act as negative control. Tissues were washed after 16–18 h in PBT/1% BSA supplemented with normal goat serum 3 times for 15 min each with constant agitation to remove unbound primary antibody. Following washes, tissues were incubated with goat anti-rabbit TRITC-conjugated secondary antibody at 1:1000 dilution (Jackson ImmunoResearch, Westgrove, PA, USA) in the dark at room temperature for 2 h. Following incubation with secondary antibody, tissue was washed 3 times in PBT/1% BSA for 15 min each time.

**Table 1. Primer sets used for RT-PCR and qPCR analysis of voltage-gated ion channel transcript expression and abundance in Malpighian tubules and anal papillae of larval *Aedes aegypti***

| Transcript | Forward sequence | Reverse sequence | NCBI accession no. | NCBI match | $T_a$ |
|---|---|---|---|---|---|
| *actin* | CAGGGTGTGATGGTCGGTAT | CGGTGTGTTGAAGGTTTCG | OR187519 | XM_001655125.2 | 60 |
| *CaV1a1×9* | TTTCCAAACCTTCCCGCAAG | CGTACTCACTCCATAGCCGA | OR187520 | XM_021844183.1 | 59 |
| *HCN2×4* | CCGTCTACTGAAAAACCATCATC | GTTCGGCGTTATCTTGTTGC | OR187523 | XM_021844343.1 | 56 |
| *TRPpainless211.2 (TRP/painless 1)* | CAGTATCCCATCCACTTTGC | CTTCCTCAACTCCCCCTTC | OR187524 | XM_001652211.2 | 58 |
| *painless473 (TRP/painless 2)* | AGTTGGTGTGGTGTTGCTTG | AAGAGAGGGCAGAAGAGTGC | OR187525 | XM_021839473.1 | 59 |
| *painless989 (TRP/painless 3)* | CCGCTTTCAACGAGAGAATC | GGACGAGTTTTTCATCAGCA | OR187526 | XM_001648989.2 | 59 |
| *TRPA1* | GCCATACTACCAGAACCATC | CGAAATCAATACCTCCTTTG | OR187527 | XM_021842764.1 | 57 |
| *TRPpyrexia (TRP/pyrexia 1)* | CGGTATTGCTGGGATGGAC | ATGAACGGAGGGTCTTTTCC | OR187529 | XM_021853484.1 | 60 |
| *TRPpyrexiaX3 (TRP/pyrexia 2)* | GCCACACACAATGCCTACAA | CACAATCCGATTTGCCCACA | OR187530 | XM_021853483.1 | 61 |
| *paraX7* | GGCGACCACAAGCAATAGTA | AACGAGACCTAAAATGGACAGGA | OR187528 | XM_021852347.1 | 58 |
| *NALCN* | CGAAACACCGCAATACAGAG | CAAGCATCGTAAAATCATCAAAAG | OR187521 | XM_021854385.1 | 59 |
| *KCNQ1* | GCCATCATCTTCATCATCACATG | GGAAGAACTCGATCGAAAACCATA | OR187522 | XM_021842612.1 | 63 |

$T_a$, annealing temperature.

Journal of Experimental Biology (2024) 227, jeb246486. doi:10.1242/jeb.246486

Tissues were then mounted on slides using a transfer pipet. Slides were then blotted dry using KimWipes and preparations were mounted using ProLong Antifade® reagent (ThermoFisher Scientific) containing 4,6-diamidino-2-phenylindole (DAPI) as a nuclear stain under coverslips and left to cure in the dark. Images of VGICs were obtained using a Nikon Eclipse CI-S microscope and Nikon DS-Qi2 camera in imaging facilities at the Department of Biological Sciences at California State University San Marcos.

Cross-section immunohistochemistry procedures were performed as follows. Tissues were carefully microdissected out in appropriate saline (see above) and fixed in Bouin's solution for 4 h at room temperature. Following fixation, all tissues were rinsed 3 times in 70% ethanol and stored in 70% ethanol at 4°C until further processing. Fixed tissues were dehydrated through an ascending series of ethanol rinses (70–100%), cleared with xylene and infiltrated and embedded in Polyfin Tissue Embedding Medium (cat. no. 50-279-84, fisher scientific). Then, 5 µm thick sections were cut using an HM 355 S rotary microtome (MICROM International GmbH, Walldorf, Germany), collected on glass slides and incubated overnight at 45°C. Sections were deparaffinized with xylene, rehydrated to water via a descending ethanol series (100% to 50%), and subjected to heat-induced epitope retrieval (HIER). HIER was accomplished by immersing slides in a sodium citrate buffer (10 mmol $l^{-1}$, pH 6.0) and heating both solution and slides in a microwave oven to 92–95°C. The solution was allowed to cool for 20 min, reheated again and cooled for a further 15 min. Slides were then washed 3 times with PBS (pH 7.4) and quenched for 30 min in 3% $H_2O_2$ in PBS. Following quenching, slides were successively washed with 0.4% Kodak Photo-Flo 200 in PBS (PF/PBS, 10 min), 0.05% Triton X-100 in PBS (PBT, 10 min), and 10% antibody dilution buffer (ADB: 10% goat serum, 3% BSA in PBT) in PBS (ADB/PBS, 10 min). Slides were incubated overnight at room temperature with one of the rabbit polyclonal anti-VGIC antibodies (anti-NALCN, anti-TRP/Painless, anti-KCNH8, or anti-$Ca_V1$; 1:100 dilution in ADB). Custom epitope affinity purified anti-VGIC antibodies (see above) were used. As negative controls, two sets of slides were also incubated overnight with ADB alone. Following overnight incubation, sections were successively washed with PF/PBS, PBT and ADB/PBS (10 min each) as described above, and incubated with tetramethylrhodamine isothiocyanate (TRITC)-labeled goat anti-rabbit antibody (1:500 in ADB; Jackson ImmunoResearch) for 2 h at room temperature. Slides were then successively washed with PF/PBS, PBT and PF/PBS (10 min each) and rinsed 3 times with 0.4% PF in distilled water (PF/$dH_2O$, 1 min each). Slides were air dried for 1 h and mounted with Molecular Probes ProLong Antifade (ThermoFisher Scientific) containing DAPI. Fluorescence images were captured using a Nikon Eclipse CI-S microscope and Nikon DS-Qi2 camera, and merged using ImageJ software (US National Institutes of Health, Bethesda, MD, USA).

Adult female mosquitoes were either fed on sucrose solution or fed on animal blood, and harvested for microscopy 4 h after feeding. Once MTs were microdissected out, tissue samples were processed as above for $Ca_V1$ immunohistochemistry (see below).

Negative control preparations with primary antibodies omitted were used with every set of IHC samples, did not produce immunofluorescence, and were omitted for brevity.

### Western blotting analysis

MTs were isolated in ice-cold physiological saline, transferred to microtubes and stored at −80°C for later analysis. Tissues from 40 larvae were combined in each tube. For examination of $Ca_V1$ expression, tissue samples were thawed on ice and homogenized in a RIPA homogenization buffer containing 50 mmol $l^{-1}$ Tris-HCl, pH 7.5, 150 mmol $l^{-1}$ NaCl, 1% sodium deoxycholate, 1% Triton X-100, 0.1% SDS, 1 mmol $l^{-1}$ PMSF and 1:200 protease inhibitor cocktail (Sigma-Aldrich). All homogenates were then centrifuged at 13,000 ***g*** for 20 min at 4°C, and the protein content of the collected supernatants was determined using the Pierce 660 nm assay (ThermoFisher Scientific) according to the manufacturer's guidelines. Samples (10–20 µg protein) were prepared for SDS-PAGE by heating for 5 min at 100°C in a 6× loading buffer containing 360 mmol $l^{-1}$ Tris-HCl (pH 6.8), 12% (w/v) SDS, 30% glycerol, 600 mmol $l^{-1}$ DTT and 0.03% (w/v) Bromophenol Blue. SDS-PAGE electrophoresis and western blot analysis of $Ca_V1$ were conducted according to a previously described protocol (Kolosov and Kelly, 2017) using anti-$Ca_V1$ antibody at a 1:1000 dilution. Antigen reactivity was visualized using SuperSignal West Pico PLUS Chemiluminescent Western ECL substrate kit (34577, ThermoScientific, Rockford, IL, USA) and images were captured using a iBright CL750 imaging system (ThermoFisher Scientific). A brightfield image of the blot was acquired to superimpose the ladder onto the final blot figure panel.

### $V_m$ measurements and $Ca_V1$ inhibitor

Larvae were dissected under larval *Ae. aegypti* saline (see recipe above). MTs together with the gut were dissected out and MTs were pulled away from the gut and separated from tracheae. MTs were excised and mounted in petri dish pre-coated with poly-L-lysine to aid tissue adherence. Transepithelial potential ($V_{te}$) and basolateral membrane potential ($V_{bl}$) were measured in separate preparations by impaling the tubule lumen with a microelectrode pulled from BF150-110-10 glass (Sutter Instruments) on a microelectrode puller PUL-1000 (World Precision Instruments, Inc.) where the barrel was filled with 150 mmol $l^{-1}$ KCl (Kolosov et al., 2021). All potentials were measured with respect to a reference electrode back-filled with 150 mmol $l^{-1}$ KCl. $V_{te}$ and $V_{bl}$ were recorded with a high impedance (>$10^{13}$ Ω) electrometer (ML165 pH Amp, ADInstruments), which in turn was connected to a PowerLab 2/26 data acquisition system running LabChart software (ADInstruments). Apical membrane potential ($V_a$) was calculated as the difference between $V_{te}$ and $V_{bl}$.

Stock solutions of nifedipine (Sigma-Aldrich), an inhibitor of voltage-gated $Ca_V1$ channels, was prepared in DMSO and diluted in saline to 0.1 µmol $l^{-1}$ (final DMSO concentration in the bath did not exceed 0.01% v/v). Addition of inhibitor to the bathing saline for $V_{te}/V_{bl}$ was achieved by replacing 1/10th of the volume of bathing saline with freshly prepared inhibitor solution at 10× the final concentration in saline. Nifedipine at concentrations used in this study did not affect the response time $V_{te}/V_{bl}$ electrodes. $V_{te}$ and $V_{bl}$ measurements were performed in different cells.

### Statistical analysis

Significance of the effect of salinity exposure on hemolymph ion concentration, and mRNA abundance of ion channels was assessed with Student's *t*-test with a significance limit of $P<0.05$, following checks for normality and homogeneity of variance (performed in GraphPad Prism 7 statistical software). The effects of pharmacological inhibition of $Ca_V1$ on basolateral and transepithelial membrane potentials were assessed using a paired *t*-test in the same software with the same significance limit.

## RESULTS

### Hemolymph ion loading in BW-exposed *Ae. aegypti* larvae

Hemolymph ion concentrations were measured to determine whether 24 h exposure to BW constituted a significant challenge

Journal of Experimental Biology (2024) 227, jeb246486. doi:10.1242/jeb.246486

to the salt-and-water balance of the larvae. Significant elevation in hemolymph [$Na^+$] and [$Cl^-$] was observed in BW-exposed larvae. Hemolymph [$Na^+$] increased significantly from 89.0±4.2 mmol $l^{-1}$ to 132.1±1.6 mmol $l^{-1}$ ($n$=9–10, $t$-test $P$<0.0001) (Fig. 1A). Hemolymph [$Cl^-$] increased significantly from 96.2 ±3.3 mmol $l^{-1}$ to 128.0±2.5 mmol $l^{-1}$ ($n$=10, $t$-test $P$<0.0001) (Fig. 1B). Hemolymph [$K^+$] did not change significantly (5.4 ±0.7 mmol $l^{-1}$ to 6.7±0.9 mmol $l^{-1}$, $n$=10, $P$=0.2822) (Fig. 1C).

### Transcriptomes of MTs of larval *Ae. aegypti* and differentially expressed transcripts following 24 h BW exposure

A preliminary literature search and survey of publicly available and collaborator transcriptomic datasets indicated that larval MTs and AP, as well as adult MTs express a variety of VGICs, which change in transcript abundance in response to salt and water imbalance (Table 2). Following this initial analysis, which was particularly useful for identifying targets in the AP of larvae, all analysis aimed at identifying targets in MTs was conducted using transcriptomic data generated in the lab.

Analysis of our own transcriptomic data detected expression of multiple voltage-gated cation-, $Na^+$-, $K^+$- and $Ca^{2+}$-selective channels, as well as many LGICs and MSICs in the MTs of larval *Ae. aegypti* (Fig. 2). VGIC assemblage in MT epithelia included: several transient receptor potential (TRP) A, M and V channels, ranging in mean abundance from 2041.66 transcripts per million (TPM) (*TRPA/pyrexia*) to 0.11 TPM (*TRPV5*); voltage-gated $K^+$ channels *KCNS1/shab*, *KCNH8/elk*, *KCNQ2*, *KCNH6/erg2*, *KCNQ1*, *KCNH1/eag* and $K_{Ca}$*5.1/slo*, ranging in abundance from 550.71 TPM (*KCNS1/shab*) to 1.00 TPM ($K_{Ca}$*5.1/slo*); voltage-gated $Na^+$ channels *nalcn* (5.11 TPM), *60E* (0.74 TPM) and *para* (1.90 TPM); voltage-gated $Ca^{2+}$ channels $Ca_V$*1* (1.60 TPM) and $Ca_V$*3* (1.60 TPM); and cation-selective *HCN2* (0.67 TPM) (see Table S1).

Deseq2 analysis of BW-exposed and FW-acclimated MT transcriptomes revealed that several VGICs altered in transcript abundance in the MT with salinity exposure. Transcripts of voltage-gated *TRP/pyrexia*, *TRP/painless 1* and *nalcn* were less abundant in the MTs of larvae exposed to BW. In contrast, voltage-gated *TRP/painless 2*, *TRP/painless 3* and *KCNH8* were all more abundant in the MTs of BW-exposed larvae (see Table S1).

In order to establish the background of salt-and-water balance transcriptome changes, alterations in transcript abundance of solute and water transporters were quantified as well. Presence and abundance changes of ion pumps, channels and transporters, as well as aquaporins, hormone receptors and transcripts encoding cyclic nucleotide and $Ca^{2+}$ signaling pathways, and septate junction proteins have been provided in the supplementary information and are not discussed in the manuscript for brevity and clarity of focus (see Table S1, ‘General transporters’).

### VGICs are expressed in the MTs and AP of larval *Ae. aegypti*

PCR and gel electrophoresis confirmed the expression of several VGICs from different ion channel families using transcript-specific primers, where most channels were found to be expressed in both MTs and AP of *Ae. aegypti* (Fig. 3). Expression of the voltage-gated calcium channel $Ca_V$*1*, the sodium channels *nalcn* and *parax7*, the potassium channel *KCNQ1*, and the transient receptor potential channels *TRPA1*, *TRP/painless 1*, *2* and *3*, as well as *TRP/pyrexia 1* and *2* was detected in both MTs and AP of *Ae. aegypti* larvae. Expression of the hyperpolarization-activated cyclic nucleotide-gated sodium/potassium channel *HCN2×4* was detected only in the MTs.

### Many VGICs expressed in MTs and AP alter in transcript abundance following 24 h BW exposure

Transcriptomics did not find any effect of BW exposure on the expression levels of VGICs – RNAseq is prone to false negatives due to a low number of replicates, low expression levels of many genes, insufficient depth of sequencing, and multiple comparison false discovery rate adjustment (e.g. Robert and Watson, 2015). Therefore, we employed qPCR to detect multiple changes in mRNA abundance between FW- and BW-exposed larvae. In AP, mRNA

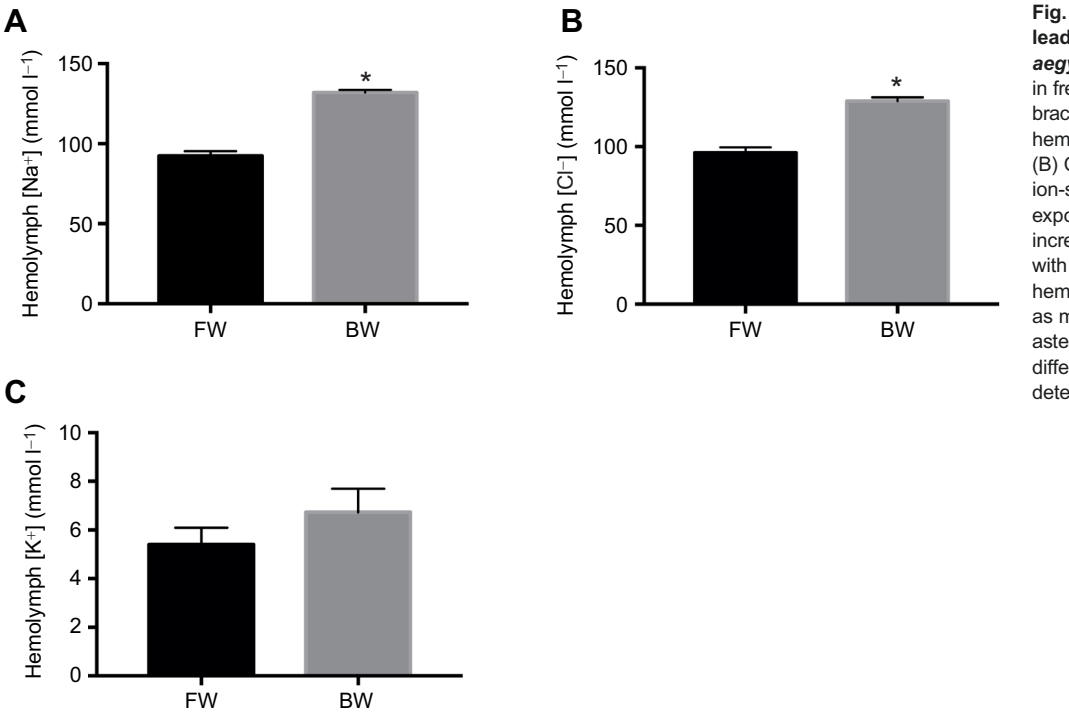


**Fig. 1. Brackish water exposure leads to ion loading in larval *Aedes aegypti*.** Larval *Ae. aegypti* were raised in freshwater (FW), exposed to brackish water (BW) for 24 h, and hemolymph concentrations of (A) $Na^+$, (B) $Cl^-$ and (C) $K^+$ were measured with ion-selective microelectrodes. BW-exposed larvae demonstrated increased hemolymph [$Na^+$] and [$Cl^-$] with no significant perturbation of hemolymph [$K^+$]. All data are presented as mean values±s.e.m. ($N$=10). An asterisk indicates a significant difference due to BW exposure as determined by Student’s $t$-test.

**Table 2. Summary of publicly available and collaborator-generated RNAseq data**

| Animal clade | Species | Tissue/organ | Differential factor | VGICs | Reference |
|---|---|---|---|---|---|
| Insects, lepidopterans | *Trichoplusia ni* | MTs | Diet (ion poor versus ion rich) | $Ca_V1$, TRPV5, CATSPER1, KCNH8 | Kolosov et al., 2019 |
| | | | Regional heterogeneity (distal versus proximal) | $Na_V$/para, $Ca_V1$–3, KCNA3, KCNC1, KCNH1 and 8, KCNH6, KCNQ1, KCNM/Slo, TRP (A,M,V) | Kolosov and O'Donnell, 2019 |
| | *Helicoverpa armigera* | MTs | Life stage (larva versus adult) | $Na_V$/Para, $Ca_V1$, CATSPER1, KCNA3, KCNC1, TRPA1, short TRP4, TRPM | Yuan et al., 2018 |
| Insects, dipterans | *Aedes albopictus* | MTs | Diet (sugar meal versus blood meal) | KCNA3, KCNH1, TRPA1/pyrexia, $K_V$ | Esquivel et al., 2014 |
| | *Aedes aegypti* | MTs | Life stage (larva versus adult) | $Ca_V1$–3, $Na_V$, KCND1, KCNC1, KCNQ1, TRP channels, HCN2, HCN4, nalcn | Li et al., 2017 |
| | | Larval AP | Salinity (freshwater versus brackish water) | $Ca_V1$, $Na_V$, KCND1, KCNQ1, TRP A, KCNA3, HCN2, HCN4, Nalcn | Durant et al., 2021 |
| Mollusks, bivalves | *Tridacna squamosa* | Gill (ctenidium) | Light exposure | $Ca_V1$ | Cao-Pham et al., 2019 |
| | *Crassostrea gigas* | Mantle epithelium | Salinity, exposure to dilute seawater | $Ca_V3$ | Sillanpää et al., 2020 |
| Teleosts, eels | *Anguilla japonica* | Gill epithelia | Environmental salinity (freshwater versus seawater) | PVC – SCN3B, $Ca_V1$, TRPA1, $H_V1$, MRC – $Ca_Va2d3$ | Lai et al., 2015 |
| | | | Cell-type heterogeneity (mitochondrion-rich versus pavement cells) | KCNE1 | |
| Mammals | *Canis lupus familiaris* | Cultured kidney epithelia | Osmolality stress | SCN1B, $Ca_V2$–3, KCNQ4, KCNC4, HCN2, TRPV1–2, TRPM6 | Rasmussen et al., 2019 |
| | | | Salt stress | SCN1B, $Ca_V3$, KCNQ4, KCNC3, HCN2, TRPC1, TRPV1–2 | |

Sample survey of publicly available raw transcriptomic data and studies citing expression of voltage-gated ion channels (VGICs) in epithelia of many animal clades. Analysis of raw transcriptomic datasets of several studies indicated that VGICs are expressed in the Malpighian tubules (MTs) of larvae and adults, as well as anal papillae (AP) of *Ae. aegypti* larvae. In particular, RNAseq analysis suggests the presence of voltage-gated $Ca^{2+}$-, $K^+$-, $Na^+$- and cation-selective channels in the osmoregulatory epithelia of *Ae. aegypti*.

abundance of *KCNQ1* and *TRP/pyrexia 1* significantly decreased ∼2-fold, while that of *nalcn* decreased ∼4-fold. *TRP/painless 2* significantly increased ∼4-fold, while *TRPA1* increased ∼2-fold in mRNA abundance following 24 h BW exposure (Fig. 4). Similarly, in MTs, voltage-gated *$Ca_V1$*, *TRP/pyrexia 2* and *TRPA1* all significantly decreased ∼2-fold in mRNA abundance, while *KCNQ1* significantly increased ∼12-fold, and *TRP/painless 1* and *TRP/painless 3* significantly increased ∼3.5-fold in mRNA abundance (Fig. 5). All *P*-values regarding data presented in Figs 4 and 5 can be found in Table S1.

### $Ca_V1$, Nalcn, KCNH8 and TRP/Painless immunolocalize to AP and MT epithelia

Immunohistochemistry was used to demonstrate that $Ca_V1$ was expressed in the luminal side of AP (Fig. 6A,B), Nalcn was expressed in the water-facing membrane (Fig. 6C,D), while KCNH8 expression was restricted to the distal-most tip of the AP (Fig. 6E,F), and TRP/Painless was expressed in the water-facing membrane of the AP (Fig. 6G,H).

In contrast, expression of all VGICs in the MTs was restricted to the apical (lumen-facing) membrane of the principal cells, which expressed Nalcn (Fig. 7A,B), TRP/Painless (Fig. 7C,D) and KCNH8 (Fig. 7E,F). Western blotting with anti-$Ca_V1$ antibody identified $Ca_V1$ as a single protein of expected molecular weight (Fig. 8A); this was detected in the MTs larvae (Fig. 8B) and sugar-fed (Fig. 8C) and blood-fed (Fig. 8D) adults.

### Pharmacological inhibition of $Ca_V1$ alters $V_{bl}$ and $V_{te}$ membrane potential in the larval and adult MTs of *Ae. aegypti*

Pharmacological inhibition of $Ca_V1$ significantly depolarized MT epithelia of adults and larvae. In larvae, $V_{te}$ decreased significantly from 29.02±1.93 mV to 20.16±2.16 mV ($P<0.001$), but $V_{bl}$ did not alter significantly (−74.20±6.77 mV to −61.40±10.51 mV) (Fig. 8E), corresponding with a calculated change in $V_a$ from approximately −103 mV to approximately −81 mV. In contrast, both $V_{te}$ and $V_{bl}$ altered in adult MTs from 41.38±6.95 mV to 15.40±4.35 mV ($P=0.015$) and from −32.28±2.19 mV to −20.28±2.05 mV ($P=0.003$), respectively, corresponding with a calculated change in $V_a$ from approximately −74 mV to approximately −36 mV.

## DISCUSSION

### Overview of findings

In the current study, we employed data mining from publicly available datasets, as well as in-lab transcriptomics to indicate the presence of VGICs in AP and MTs of larval *Ae. aegypti*. We then used acute salinity exposure combined with PCR and gel electrophoresis, qPCR, immunohistochemistry and $V_m$ measurements to directly demonstrate the presence of VGICs in osmoregulatory epithelia of larval *Ae. aegypti* and their potential relevance to salt and water balance in MTs and AP. An acute exposure to increased salinity presented a challenge in osmoregulatory function, as demonstrated by ion loading of the hemolymph. A hypothesis-generating, transcriptomic approach was used to find VGIC genes that might be involved in ion transport and its regulation in the MTs and AP of larval mosquitos, and suggested that multiple VGICs belonging to several ion channel families were expressed in these osmoregulatory organs (Table 2, Fig. 2). Using PCR and gel electrophoresis, we confirmed that voltage-gated $Ca^{2+}$, cation-selective, $Na^+$ and $K^+$ channels are expressed in both MTs and AP (Fig. 3). Additionally, to investigate the abundance of VGIC transcripts in a quantitative manner, we determined that in BW-exposed larvae, *KCNQ1* (∼2-fold), *nalcn* (∼4-fold) and *TRP/pyrexia 1* (∼2-fold) demonstrated lower mRNA abundance in AP (Fig. 4), while *$Ca_V1$* (∼2-fold), *Nalcn* (∼3-fold), *TRP/pyrexia 2* (∼2-fold) and *TRPA1* (∼4-fold) were lower in mRNA abundance in the MTs (Fig. 5). In

Journal of Experimental Biology (2024) 227, jeb246486. doi:10.1242/jeb.246486

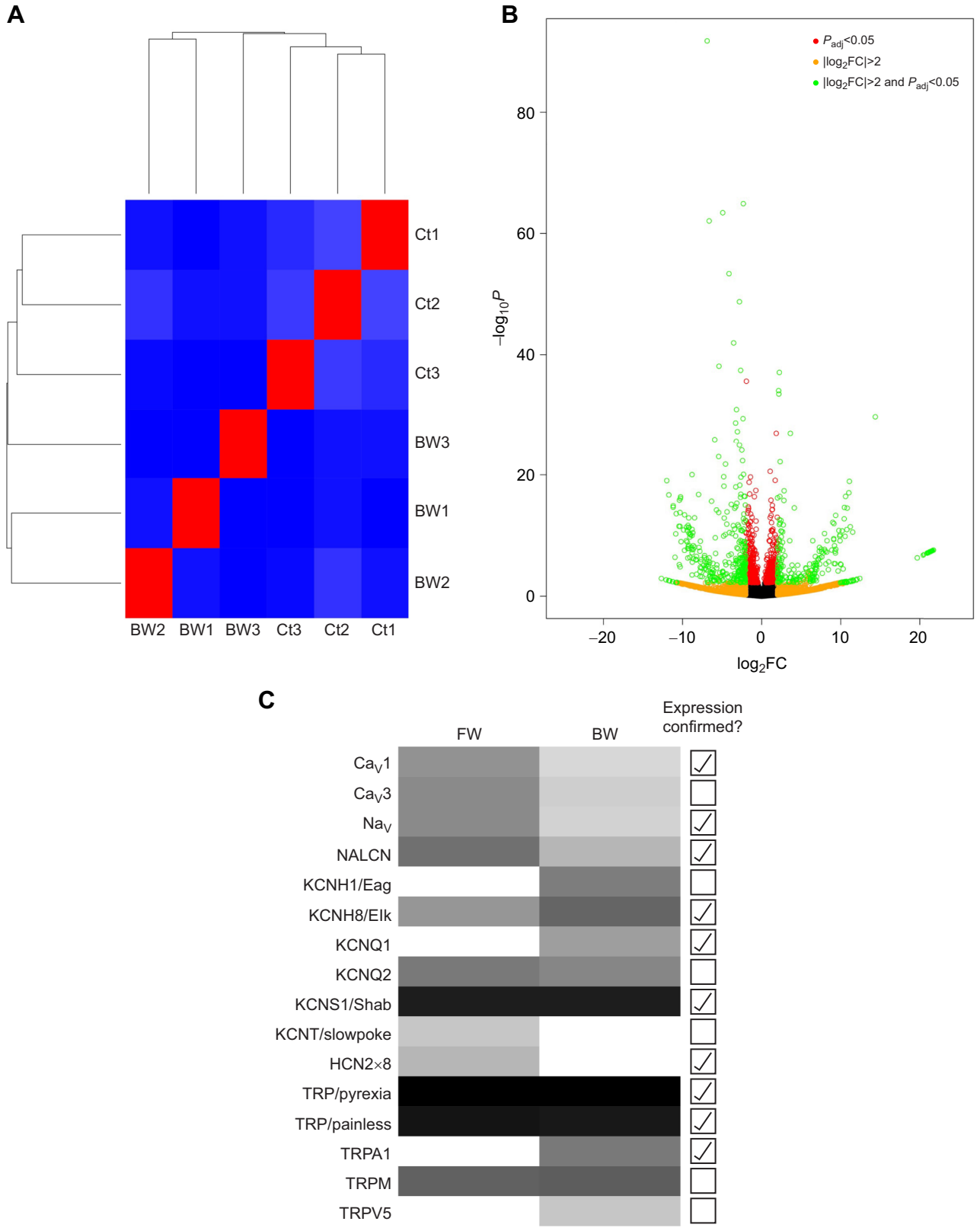


**Fig. 2. Summary of lab-generated RNAseq data for the current study.** (A) Clustering and heatmap of Malpighian tubule (MT) replicate samples of FW-reared and BW-exposed *Ae. aegypti* larvae demonstrating that when analyzed for all gene expression, FW (Ct1–3) and BW (BW1–3) samples cluster with replicates from their respective groups. (B) Volcano plots show differential expression of individual transcripts as determined by the fold-change (FC) in Deseq2 analysis in R plotted against the *P*-value of the change and is indicated logarithmically as $\log_2$FC in yellow when $|\log_2 FC|>2$. Changes with *P* adjusted for the false discovery rate ($P_{adj}$)<0.05 are indicated in red. Changes in green indicate both $|\log_2 FC|>2$ and $P_{adj}<0.05$. (C) Heatmap of voltage-gated ion channel expression in the MTs of FW-reared and BW-exposed larvae. Expression of select voltage-gated ion channels (VGICs) confirmed by at least one more method in the current study is indicated.

Journal of Experimental Biology (2024) 227, jeb246486. doi:10.1242/jeb.246486

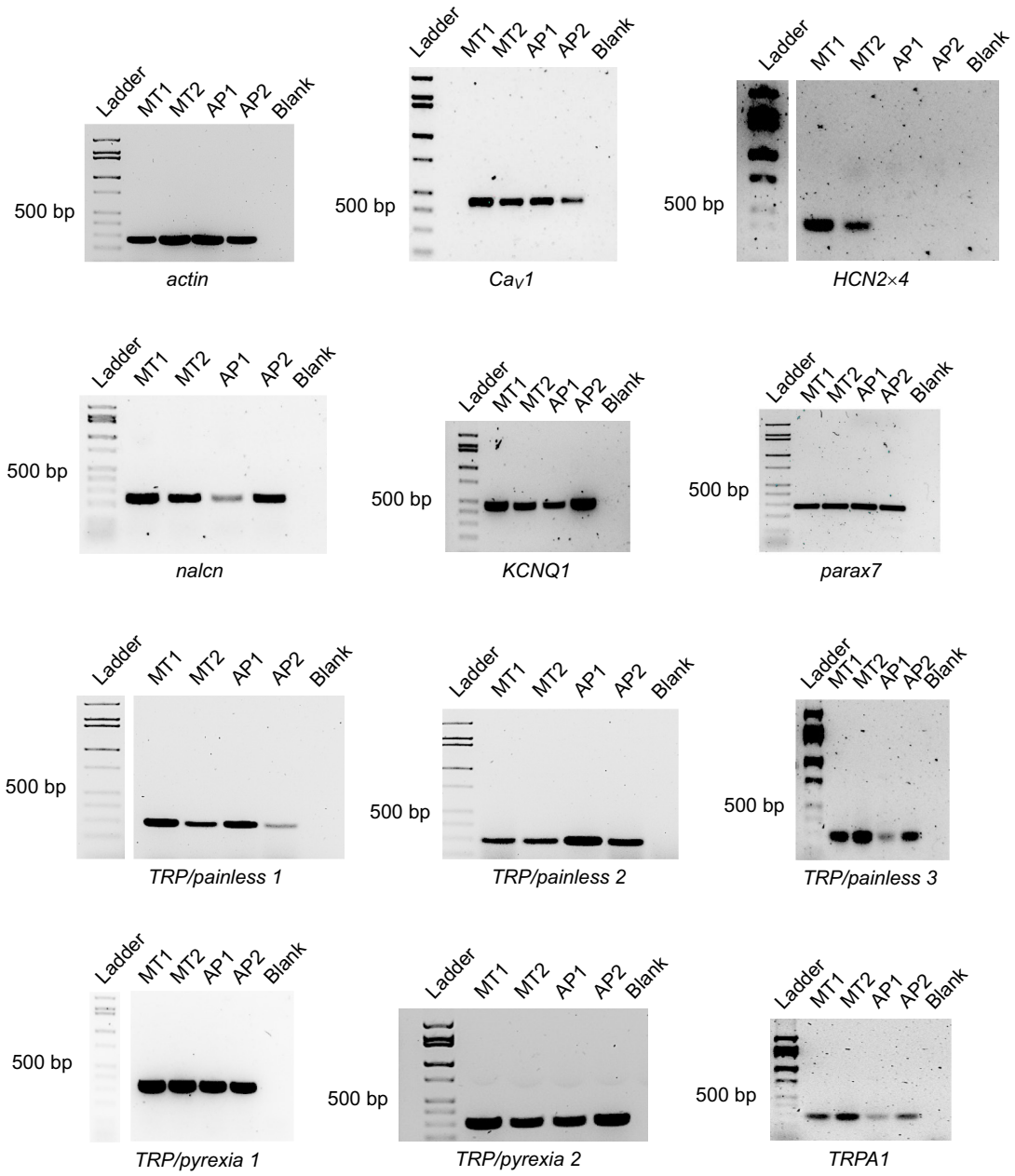


**Fig. 3. VGICs are expressed in MTs and anal papillae (AP) of larval *Ae. aegypti*.** RT-PCR detection of transcripts encoding *Aedes* VGICs; *actin* RT-PCR was used as positive control. Negative control (no template) in every PCR was also loaded onto the gel (blank). The 500 bp marker is indicated (ladder) for reference and all bands below it decrease by 100 bp. Two replicates were used to minimize false negatives.

contrast, BW exposure upregulated *TRP/painless 2* (~4-fold) and *TRPA1* (~2-fold) in AP (Fig. 4), and *KCNQ1*, *TRP/painless 1* and *TRP/painless 3* (~3.5-fold) in MTs (Fig. 5). We used immunolocalization to confirm the protein products of target VGICs are in the osmoregulatory epithelia, and found luminal $Ca_V1$, water-facing Nalcn and TRP/Painless, and distal KCNH8 in AP epithelia (Fig. 6), and all four VGICs in the apical (luminal) membrane of principal cells in MT epithelia (Fig. 7). Of special interest was the pharmacological inhibition of $Ca_V1$ in larval and adult MTs, in agreement with previous studies on larval lepidopterans, which led to depolarization of $V_{te}$ in larvae and adults, as well as depolarization of $V_{bl}$ in adults only (Fig. 8). These data bring forth evidence of the presence of VGICs in non-innervated, non-contractile epithelia of mosquito larvae, and their functional relevance to the regulation of epithelial ion transport and salt and water balance of the animal. Whether detected VGICs directly participate in directional ion transport and/or setting of $V_m$ in MTs and AP of larval mosquitoes, or whether they are simply used respond to $V_m$ changes preceding the reactionary change in ion transport (e.g. environmental, or systemic ion levels that epithelia are exposed to, or mechanosensation cues) will require further mechanistic study.

### Ion loading and general transcriptomic changes in the MTs of BW-exposed larvae

VGICs may provide a mechanism for rapidly adjusting ion transport in MTs and AP. In *Ae. aegypti*, ion transport in MTs and AP can alter quite rapidly with salinity exposure (Wigglesworth, 1933; Donini et al., 2007; Surendran et al., 2018a,b). Changes in ultrastructure, ion

Journal of Experimental Biology (2024) 227, jeb246486. doi:10.1242/jeb.246486

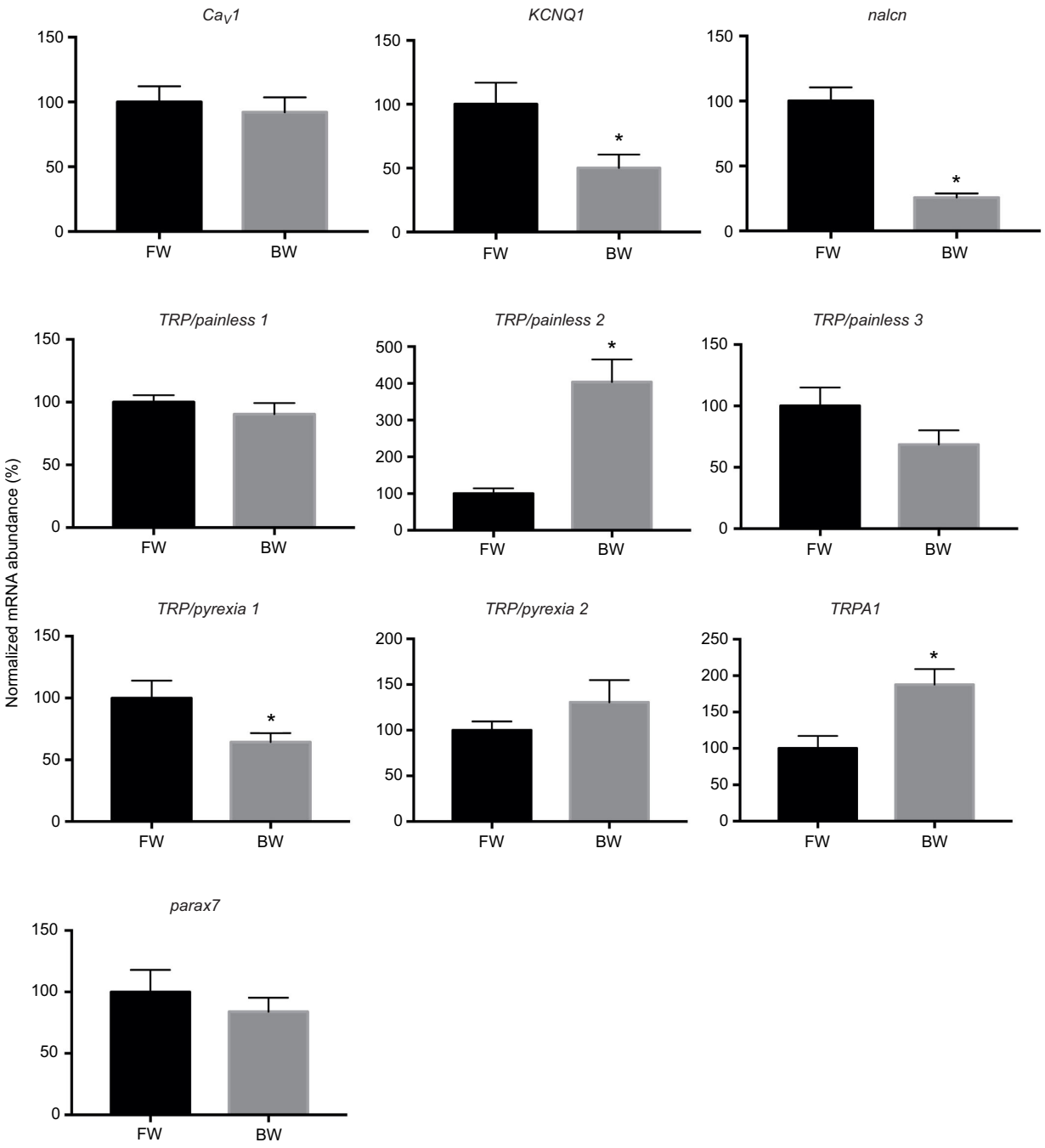


**Fig. 4. Transcript abundance of several VGICs altered significantly in the AP of larvae following 24 h exposure to BW.** Transcript abundance of *KCNQ1*, *Nalcn*, *TRP/painless 2*, *TRP/pyrexia 1* and *TRPA1* changed in the AP of *Ae. aegypti* exposed to BW for 24 h. All data are presented as mean values±s.e.m. (*N*=5–6). An asterisk indicates a significant difference due to BW exposure as determined by Student's *t*-test against the FW group.

and water transport needed to compensate for passive diffusional ion loss in the hypo-osmotic medium of FW are minimized in favor of iso-osmotic BW needs of the animal (Durant et al., 2021; Ramasamy et al., 2021). MTs of BW-exposed *Ae. aegypti* secrete less $K^+$ but the same amount of $Na^+$ (Donini et al., 2006). In general, fluid secretion by the MTs is regulated by hormones (e.g. kinin, CAPA) and the intracellular second messengers $Ca^{2+}$ and cyclic nucleotides (Donini et al., 2006). Similarly, AP in BW-exposed larvae reduce $Na^+$ and $Cl^-$ uptake from FW following 6 h of BW exposure (Donini et al., 2007).

Increased hemolymph levels of $Na^+$ and $Cl^-$ in BW-exposed larvae with no significant change in $K^+$ are in line with previous reports of acute BW exposure of freshwater obligate mosquito larvae (Patrick and Bradley, 2000; Patrick et al., 2001; Donini et al., 2006, 2007). Ion loading of the hemolymph has been shown to lead to changes in ions used in diuresis. Alterations of $K^+$ transport may be utilized to either conserve $Na^+$ under FW ($Na^+$-deprived) conditions or eliminate more $Na^+$ in saline ($Na^+$-rich) conditions (Donini et al., 2006). Simply put, the use of more $K^+$ to draw water osmotically into MTs (which may require alterations in $K^+$ transport mechanisms) spares hemolymph $Na^+$ from being lost during diuresis.

General transcriptomic response of larval MTs to BW exposure indicate significant restructuring of ion transport machinery and its

Journal of Experimental Biology (2024) 227, jeb246486. doi:10.1242/jeb.246486

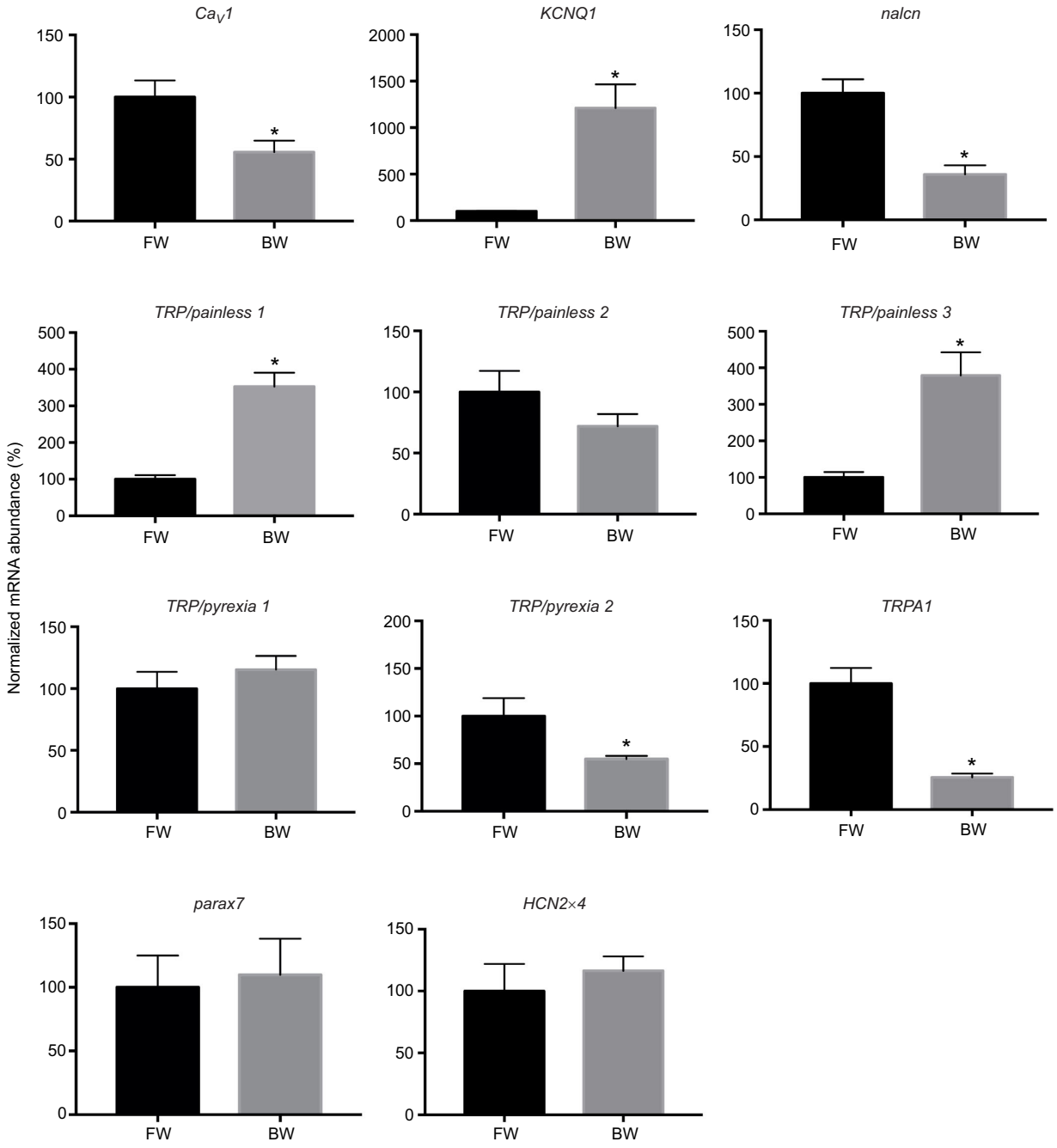


**Fig. 5. Transcript abundance of several VGICs altered significantly in the MTs of larvae following 24 h exposure to BW.** Transcript abundance of *$Ca_V1$*, *KCNQ1*, *Nalcn*, *TRP/painless 1*, *TRP/painless 3*, *TRP/pyrexia 2* and *TRPA1* changed in the MTs of *Ae. aegypti* exposed to BW for 24 h. All data are presented as mean values±s.e.m. (*N*=5). An asterisk indicates a significant difference due to BW exposure as determined by Student's *t*-test against the FW group.

regulation. The roles of many of these proteins (e.g. V-type $H^+$-ATPase, aquaporins, cyclic nucleotide and $Ca^{2+}$ signaling, septate junctions) in ion and fluid secretion by MTs of insects are well established (e.g. Patrick et al., 2006; Piermarini et al., 2010; Piermarini and Gillen, 2015; Piermarini et al., 2017a,b; Misyura et al., 2020; Duong et al., 2022; Donini et al., 2006; Beyenbach et al., 2009; Ionescu and Donini, 2012; Tiburcy et al., 2013; Efetova et al., 2013; Gioino et al., 2014; Sajadi et al., 2018; Weng et al., 2008; Calkins and Piermarini, 2017; Jonusaite et al., 2017; Kolosov et al., 2018b). However, to the best of our knowledge, much less is known about the specific roles of many hormones and signaling pathways (e.g. GRK and MAPKK) in the regulation of ion transport in larval mosquitoes (readers interested in these are directed to Table S1 for further details).

### Multiple VGICs that are expressed in MTs and AP epithelia alter in transcript abundance following exposure to BW

In line with previous transcriptomic studies on osmoregulatory epithelia of other insects, multiple VGICs were detected in the MTs and AP of larval *Ae. aegypti* (Kolosov et al., 2019; Kolosov and O'Donnell, 2019; Kapoor et al., 2021; Durant et al., 2021). In the MTs of larval lepidopterans, $Ca_V1$ and HCN1 channels have been shown to regulate cation transport – both classes of VGICs are

Journal of Experimental Biology (2024) 227, jeb246486. doi:10.1242/jeb.246486

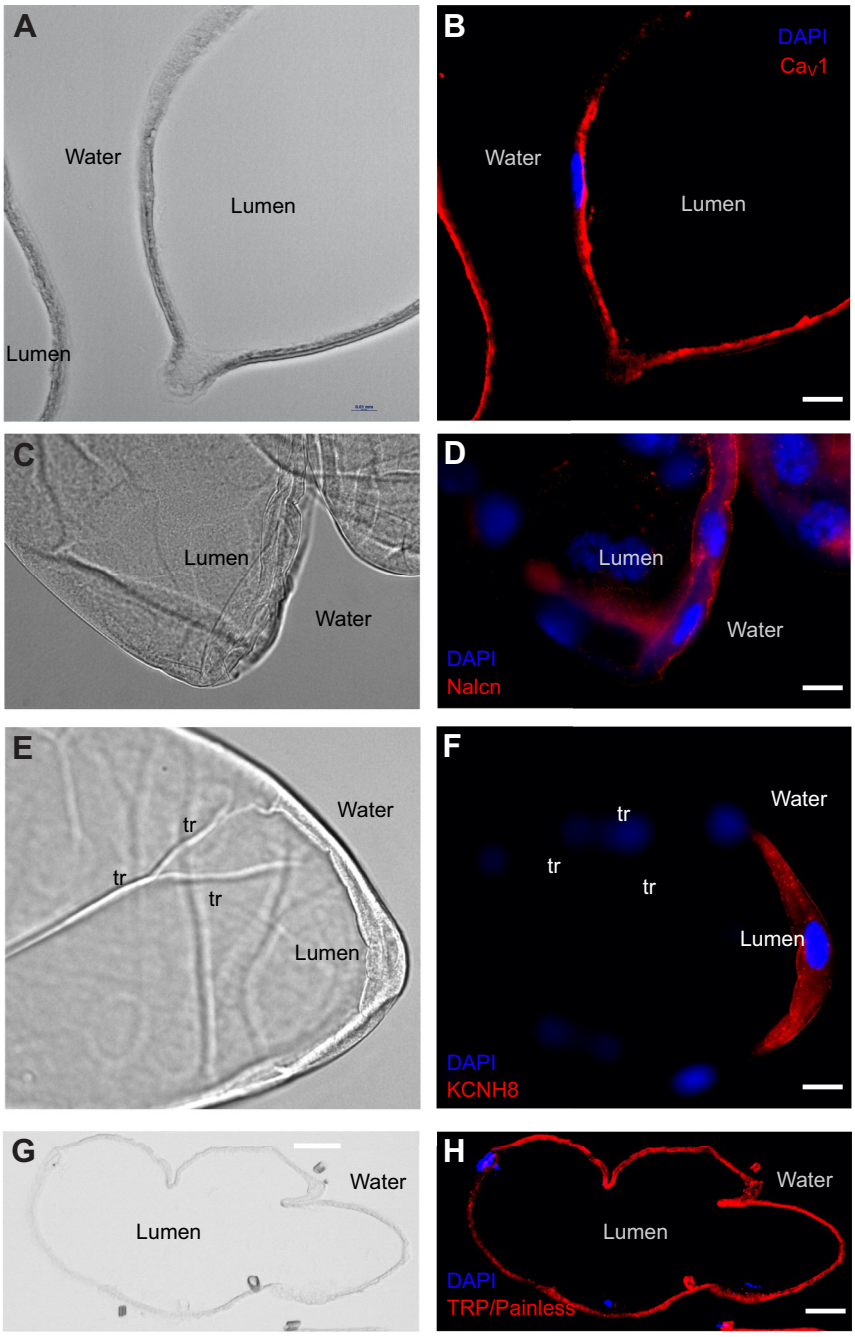


**Fig. 6. Immunolocalization of select VGICs in the AP of larval *Ae. aegypti*.** (A,B) Paraffin-embedded sections through the longitudinal plane demonstrate basolateral (luminal) $Ca_V1$ staining in AP. (C,D) Whole-mount immunohistochemistry shows Nalcn to be expressed in the apical (water-facing) membrane of AP. (E,F) Whole-mount immunohistochemistry showing localization of KCNH8 to the distal-most region of the AP. (G,H) Paraffin-embedded sections through the transverse plane demonstrate apical (water-facing) membrane localization of TRP/Painless. A–H are representative images (left, brightfield; right, immunostaining). The VGIC of interest is stained in red, nuclear DAPI staining can be seen in blue. Scale bars: A,B,G,H, 30 µm; C–F, 20 µm. tr, tracheae.

activated by changes in $V_m$, while HCN channels are additionally gated by cyclic nucleotides. Thus, the presence of these VGICs in MTs and AP of *Ae. aegypti* larvae may provide an additional connection of ion transport with $Ca^{2+}$ levels, cyclic nucleotide levels and $V_m$.

Two types of previously undescribed channels were detected in AP and/or MTs in the current study but did not alter in mRNA abundance following BW exposure – *HCN2* and *para*. HCN channels, permeable to both $Na^+$ and $K^+$, are unique among VGICs in that they have a reverse voltage dependence that leads to activation upon hyperpolarization and are additionally activated by cyclic nucleotides, where the latter overrides the former (Wahl-Schott and Biel, 2009). Cyclic nucleotides are known to enhance and reduce fluid secretion in the MTs of larval and adult *Ae. aegypti*, respectively (Donini et al., 2006; Sajadi et al., 2018). HCN channels can provide an additional link between direct activation of ion transport and second messenger-based hormone action. In larval *Trichoplusia ni*, when HCN1 channels are blocked in MTs, ion transport switches direction from $K^+$ secretion to $K^+$ reabsorption (Kolosov et al., 2019). Thus, HCN2 channels in *Ae. aegypti* may also be connected with the regulation of ion transport, which will require further detailed investigation.

*para* (short for *paralytic*) is a gene encoding a voltage-activated $Na^+$ channel of insects (Warmke et al., 1997). Functional voltage-gated $Na^+$ channels have been described in other animal epithelia, e.g. human intestinal epithelia, MTs of caterpillars (Barshack et al., 2008; Kolosov and O'Donnell, 2019). The presence of voltage-dependent $Na^+$ channels in the MTs and AP may provide a rapid link between $V_m$ and $Na^+$ permeability in these osmoregulatory epithelia.

Journal of Experimental Biology (2024) 227, jeb246486. doi:10.1242/jeb.246486

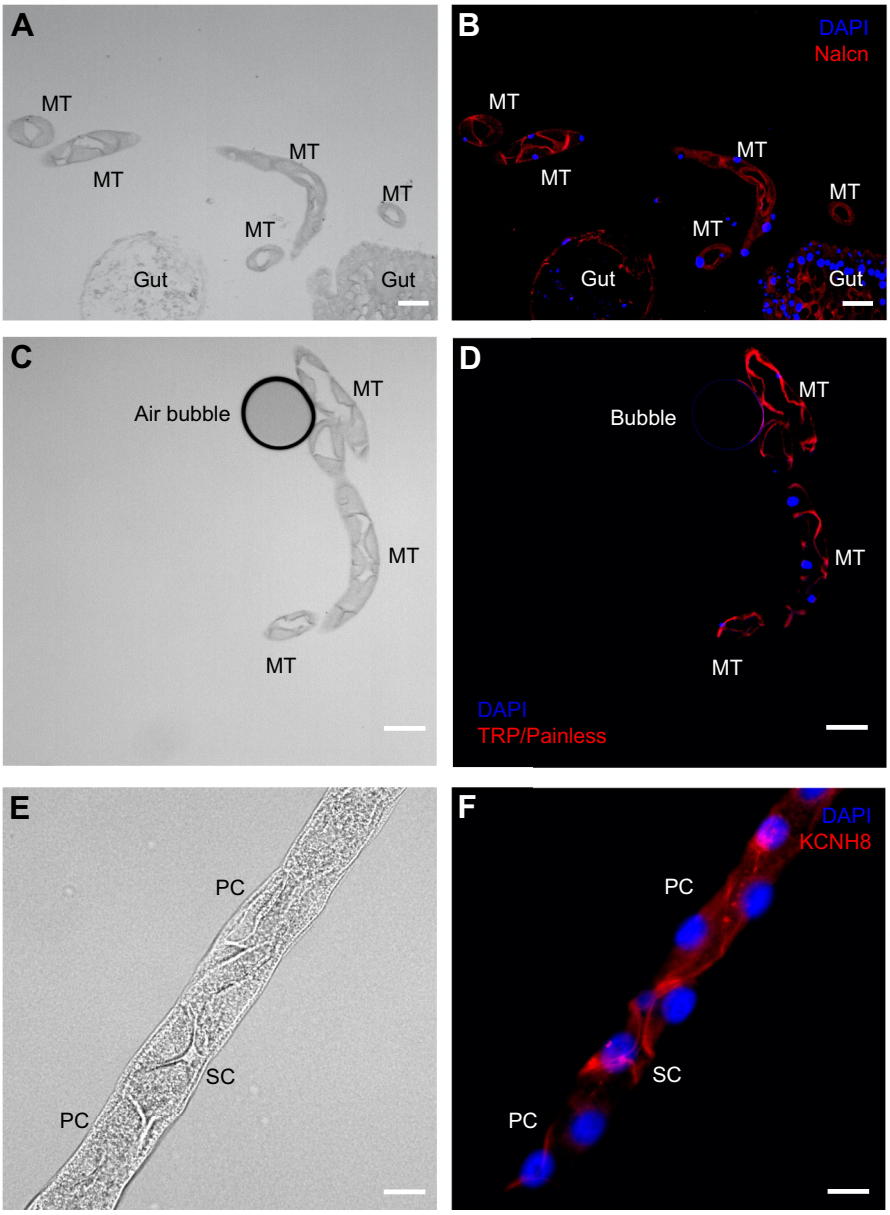


**Fig. 7. Immunolocalization of select VGICs in the MTs of larval *Ae. aegypti*.** (A–D) Paraffin-embedded sections through the longitudinal plane demonstrate apical (luminal) staining of (A,B) Nalcn and (C,D) TRP/Painless in MTs. (E,F) Whole-mount immunohistochemistry showing apical (luminal) localization of KCNH8. A–F are representative images. The VGIC of interest is stained in red, nuclear DAPI staining can be seen in blue. Scale bars: A,B, 100 µm; C,D, 60 µm; E,F, 40 µm. PC, principal cell; SC, secondary cell. Scale bars: **30 µm.**

### Apically located voltage-gated $Ca_V1$ channel may regulate ion transport in the MTs of larval and adult *Ae. aegypti*

Of special interest is the presence of $Ca_V$ channels in the MTs – these channels are key transducers of $V_m$ changes into intracellular $Ca^{2+}$ concentration changes that initiate intracellular physiological response (Catterall, 2011). At highly polarized $V_m$, $Ca_V1$ channels are normally closed. They are activated (opened) at depolarized $V_m$, allowing $Ca^{2+}$ into the cell and initiating an intracellular response. Intracellular $Ca^{2+}$ is a diuretic second messenger in insect MTs. In MTs of larval *T. ni*, $Ca_V1$ channels have been shown to connect cation transport with $V_m$ via $Ca^{2+}$ signaling (Kolosov et al., 2021). Pharmacological inhibition of $Ca_V1$ channels in the MTs of larval and adult *Ae. aegypti* in the current study had a similar effect on $V_m$, depolarizing $V_{te}$, to the previously published data in larval *T. ni* (Kolosov et al., 2021). Interestingly, in larval MTs, $V_{te}$ decreased significantly without accompanying changes in $V_{bl}$, indicating that most of the measured membrane potential change may have taken place in the apical membrane. In contrast, in adults, both $V_{bl}$ and $V_a$ seemed to have contributed to the measured changes in $V_{te}$, offering potential insight into which transporters (apical and/or basolateral) may be regulated by $Ca_V1$.

### KCNQ1 channel is downregulated in AP and upregulated in MTs of BW-exposed larvae

KCNQ/$K_V7$ channels are found in several animal epithelia, including human airway epithelial cells (Mondejar-Parreño et al., 2020), intestinal epithelia (Preston et al., 2010) and kidney (Abbott, 2015), where they are connected with transepithelial $K^+$ transport and the generation and maintenance of resting $V_m$ and ionomotive driving force (Demolombe et al., 2001). KCNQ channels are unique in the way that they can be modulated to lose their voltage dependence and remain constitutively active, are inhibited by external $K^+$ and can be modulated by intracellular $Ca^{2+}$ and cAMP levels (Schroeder et al., 2000; Abrahamyan et al., 2023; van der Horst et al., 2020). There are pronounced differences

Journal of Experimental Biology (2024) 227, jeb246486. doi:10.1242/jeb.246486

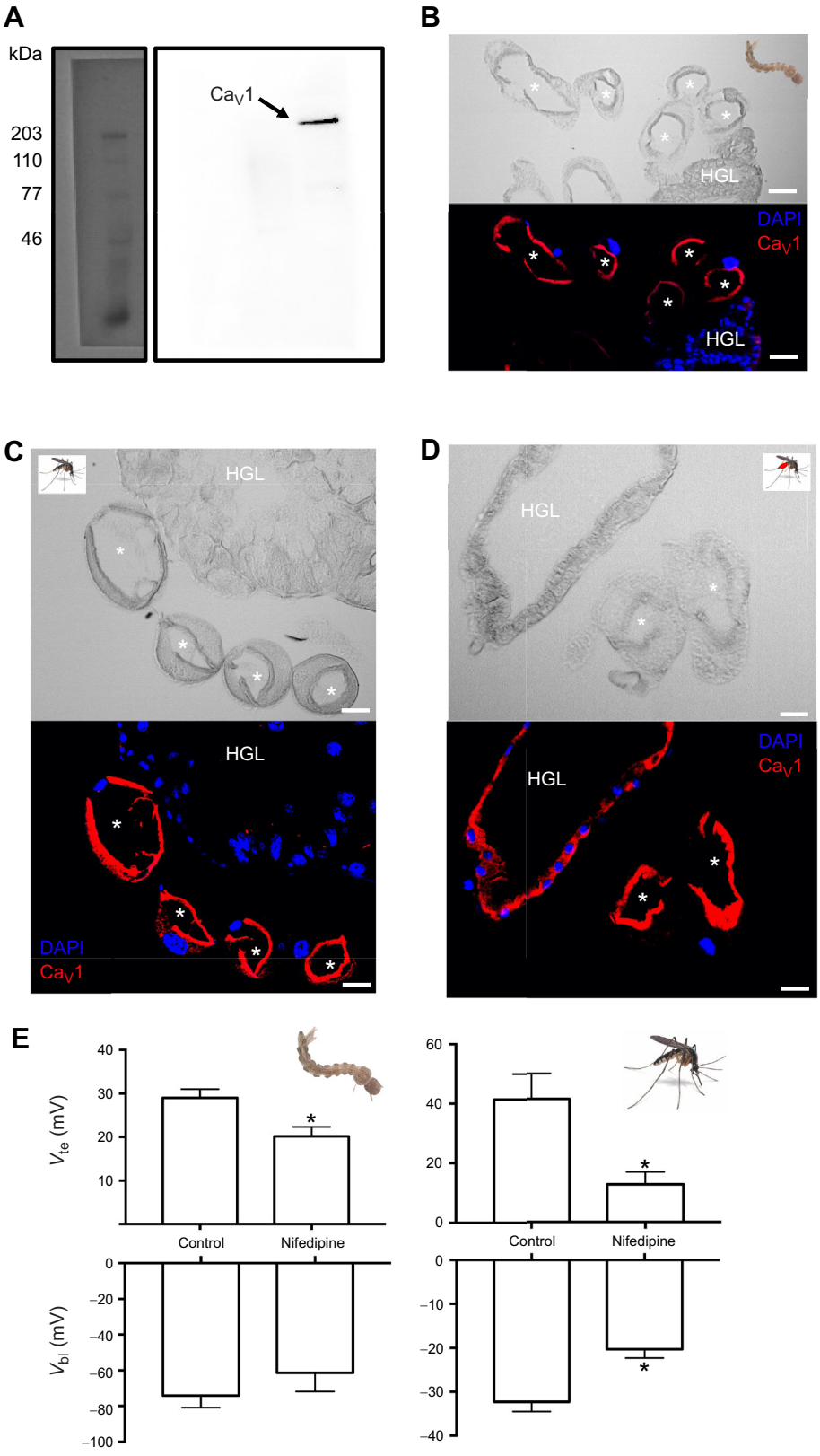


**Fig. 8. Voltage-gated calcium channel $Ca_V1$ is expressed in the apical membrane of principal cells in the MTs of *Ae. aegypti* larvae and adults, where its inhibition leads to membrane depolarization.** (A) Western blotting showing immunoreactivity of $Ca_V1$ in a representative larval MT homogenate. (B–D) Paraffin-embedded sections through the transverse plane demonstrate apical (lumen-facing) localization of $Ca_V1$ in the MTs of (B) larvae, (C) sugar-fed adults and (D) blood-fed adults. Note the increased $Ca_V1$ signal in the hindgut (HGL, hindgut lumen). (E) Pharmacological inhibition of $Ca_V1$ with nifedipine resulted in depolarization of transepithelial membrane potential ($V_{te}$) in larvae and adults, as well as depolarization of basolateral membrane potential ($V_{bl}$) in adults. Asterisks indicate MT lumen in B–D, and a significant difference due to $Ca_V1$ inhibition in E, as determined by Student's *t*-test against the control group.

in $K^+$ transport by the MTs of FW- and BW-reared *Ae. aegypti* larvae, which are thought to be aimed at conserving $Na^+$ levels in the hemolymph (Donini et al., 2006). *KCNQ1* mRNA is more abundant in MTs of BW-exposed larvae and AP of FW-reared larvae. Thus, the KCNQ1 channel may contribute to $K^+$ secretion in the MTs of BW larvae, helping the larvae rid themselves of extra $K^+$ and preventing $K^+$ loading with BW exposure. Additionally, it may contribute to the uptake of environmental $K^+$ by the AP of larvae in FW, aiding larvae in retention of hemolymph $K^+$ in the face of diffusional $K^+$ loss to FW.



Journal of Experimental Biology

### $Na^+$ leak channel Nalcn is downregulated in MTs and AP of BW-exposed larvae

MTs of FW-reared larvae produce the same amount of fluid with the same amount of $Na^+$ to BW-reared larvae, while AP actively take up more environmental $Na^+$ from surrounding FW (Donini and O'Donnell, 2005; Donini et al., 2006). Previous research has also shown that $Na^+$ is absorbed by the AP from surrounding FW with the help of electrodiffusive entry using inside-negative apical membrane potential (Edwards, 1983), which later was shown to involve V-type $H^+$-ATPase (Patrick et al., 2006) and $Na^+$ channels (Del Duca et al., 2011) in the apical (water-facing) membrane of AP. This specifically agrees with a previous study by Del Duca et al. (2011), who showed that a $Na^+$ channel blocker phenamil stops $Na^+$ uptake but that a $Na^+/H^+$ exchanger blocker [5-(*N*,*N*-hexamethylene)-amiloride] does not. Nalcn identified in this study can contribute to channel-based absorption of $Na^+$ from FW by AP. How exactly Nalcn contributes to $Na^+$ secretion in the MTs will require further detailed study. Alternatively, it may not participate in directional $Na^+$ transport in the MTs, and instead serve as a $Na^+$ sensor, contributing to the maintenance of $V_m$ and connecting it to $Na^+$ transport. In general, Nalcn is a VGIC selective for monovalent cations ($Na^+$ and $K^+$) expressed in excitable and non-excitable tissues (e.g. pancreatic β cells) (Monteil et al., 2023; Swayne et al., 2010; Xie et al., 2020). Heterozygous Nalcn knockout mice demonstrate increased blood [$Na^+$] with a possible association between Nalcn and $K^+$ excretion in humans (Sinke et al., 2011; Kho et al., 2020).

### TRP channel mRNA abundance is altered in MTs and AP of BW-exposed larvae

All six TRP channels detected in MTs and AP of larval *Ae. aegypti* belong to the TRPA channel subfamily. mRNA abundance of every TRP channel in the current study was significantly different between FW-reared and BW-exposed larvae in at least one of the examined tissues. TRP channels are cation-permeable ($Na^+$, $K^+$, $Ca^{2+}$) voltage-dependent channels (Yue and Xu, 2021). TRP channels are activated through a range of gating mechanisms ($V_m$ depolarization, ligands, etc.) (Venkatachalam and Montell, 2007). TRPA channels demonstrate wide tissue expression profiles (Cheng and Zheng, 2021), connecting them to the function of many excitable and non-excitable tissues, e.g. nerve endings of human urothelium (Vanneste et al., 2021); human lung epithelia (Ko et al., 2020), non-neuronal pancreatic islet cells, airway epithelia, and skin epidermis (Nilius et al., 2012), where it has been connected with inflammatory and cytokine release; and enteroendocrine cells of pig gut and *Drosophila* gut epithelia (Van Liefferinge et al., 2020; Gong et al., 2023). In human and rat colonic mucosa, TRPA1 has been connected with ion secretion (Talavera et al., 2020).

TRPA channels have been detected in MTs of *T. ni* (Kolosov et al., 2019), *Pieris rapae* (Mao et al., 2020) and *Bactrocera dorsalis* (Su et al., 2018). TRPA1, TRP painless and TRP pyrexia are more permeable to $K^+$ than to $Na^+$, with well-established roles in nociception and thermotaxis in excitable tissues (Tracey et al., 2003; Lee et al., 2005; Corfas and Vosshall, 2015). In contrast, and to the best of our knowledge, the roles of TRP channels in epithelia of MTs and AP have not been explored to date.

### Significance and future directions

*Aedes aegypti* is an obligate FW mosquito. Increased appearance of *Aedes* larvae in coastal BW regions worldwide in recent years is a concern in terms of the increased spread of arboviral diseases (Lee et al., 2019; Surendran et al., 2018b). *Aedes aegypti* completing their life cycle in BW may provide a perennial reservoir of arboviral transmission during dry seasons worldwide (Surendran et al., 2018b). This trend has been exacerbated by global climate change (Ramasamy and Surendran, 2012). The genomic and physiological basis of salinity adaptation and blood feeding, as well as short-term exposure to changing salinity in coastal waters are just beginning to be explored by the scientific community (Esquivel et al., 2016; Li et al., 2017; Ramasamy et al., 2021; Durant et al., 2021). Completing their life cycle in BW is advantageous as it presents larvae with an opportunity to relax osmotic/ionic stress. Acute exposure to BW, however, does require adjustment of the osmoregulatory apparatus, and thus constitutes osmoregulatory stress.

Larvae living in water of rapidly changing salinity may benefit from having a mechanism in their excretory tissues for rapidly detecting such a change. Bioelectrical signals govern the cell biology of all tissues, including non-excitable tissues, playing important roles in processes such as regeneration and ion transport (McLaughlin and Levin, 2018; Kapoor et al., 2021). Studies on animal epithelia have reported expression of $Ca^{2+}$-, $Na^+$- and $K^+$-selective, as well as non-selective and cation-permeable VGICs in epithelia of the lung, intestine (Barshack et al., 2008), kidney (Siroky et al., 2017) and skin (Pitt et al., 2021). Many of these channels are connected with intracellular $Ca^{2+}$ signaling, osmotic stress response, extracellular ion sensing and modulation of directional ion transport (Abbott, 2015; Bleich and Warth, 2000; Demolombe et al., 2001; Morera et al., 2015; Nilius and Droogmans, 2001; Schönherr et al., 2000; Shi et al., 1997; Siroky et al., 2017; Yang and Cui, 2015; Zhu et al., 2010; Kolosov et al., 2021). The presence of VGICs in epithelia may provide a mechanism for the rapid detection of depolarizing stimuli (e.g. mechanosensation of fluid flow, changing ion concentrations) that leads to changes in $V_m$. MT epithelia of larval lepidopterans (Kolosov et al., 2019; Kolosov and O'Donnell, 2019) and mosquito larvae (current study) have been shown to express high levels of mechanosensitive Piezo channels, which activate in response to membrane stretch. Their activation may allow for the activation of VGICs, and amplification of the signal via TRP channels.

VGICs of mosquitoes are often targeted with insecticides, repellents and anti-feedants because of their established role in excitable tissues of insects (Salgado, 2017; Mack et al., 2021; Inocente et al., 2018). However, the presence of VGICs in the excretory and osmoregulatory epithelia of larvae and adults is rarely considered. VGICs in osmoregulatory epithelia may provide mosquito larvae with a mechanism for rapidly sensing systemic and environmental disturbances in salt and water content. Detailed examination of what every class of VGICs does in the mosquito MTs and AP will require mechanistic study. Some VGICs may directly participate in directional ion transport, whereas others may act as ion sensors or $V_m$ setters. Whether VGICs remain voltage sensitive when expressed in non-excitable epithelia will require further mechanistic study using heterologous expression models.

#### Acknowledgements

The authors would like to thank Holly Clark and Clay Clark at IIGB Genomics Core at University of California, Riverside for synthesizing RNAseq libraries and completing sequencing.

#### Competing interests

The authors declare no competing or financial interests.

### Author contributions

Conceptualization: S.F., D.K.; Methodology: S.F., J.D., N.R., H.H.-B., D.K.; Software: D.K.; Validation: D.K.; Formal analysis: S.F., J.D., N.R., H.H.-B., D.K.; Investigation: S.F., J.D., N.R., H.H.-B., D.K.; Resources: D.K.; Data curation: S.F., J.D., N.R., H.H.-B., D.K.; Writing - original draft: S.F., D.K.; Writing - review & editing: S.F., J.D., D.K.; Visualization: S.F., J.D., N.R., H.H.-B., D.K.; Supervision: D.K.; Project administration: D.K.; Funding acquisition: D.K.

### Funding

S.F. and some material costs were supported by the National Institutes of Health/National Institute of General Medical Sciences U-RISE under award number 5T34GM136481. J.D. and some material costs were supported by the National Institutes of Health/National Institute of General Medical Sciences B2PhD program under award number T32GM146604. H.H.-B. and some material costs were supported by the National Science Foundation Research Experiences for Undergraduates (REU) program under award number 1852189. N.R. was supported by the National Institutes of Health/National Institute of General Medical Sciences Bridges to the Baccalaureate under award number 3R25GM066341. The majority of the work was supported by the startup and internal funds provided by California State University to D.K. Deposited in PMC for release after 12 months.

### Data availability

RNAseq data are deposited in SRA BioProject (PRJNA1068135).

### ECR Spotlight

This article has an associated ECR Spotlight interview with Serena Farrell.

### References

**Abbott, G. W.** (2015). Biology of the KCNQ1 potassium channel. *New J. Sci.* **2014**, 237431. doi:10.1155/2014/237431

**Abrahamyan, A., Eldstrom, J., Sahakyan, H., Karagulyan, N., Mkrtchyan, L., Karapetyan, T., Sargsyan, E., Kneussel, M., Nazaryan, K., Schwarz, J. R. et al.** (2023). Mechanism of external $K^+$ sensitivity of KCNQ1 channels. *J. Gen. Physiol.* **155**, e202213205. doi:10.1085/jgp.202213205

**Akhter, H., Misyura, L., Bui, P. and Donini, A.** (2017). Salinity responsive aquaporins in the anal papillae of the larval mosquito, *Aedes aegypti*. *Comp. Biochem. Physiol. A Mol. Integr. Physiol.* **203**, 144-151. doi:10.1016/j.cbpa.2016.09.008

**Barshack, I., Levite, M., Lang, A., Fudim, E., Picard, O., Ben Horin, S. and Chowers, Y.** (2008). Functional voltage-gated sodium channels are expressed in human intestinal epithelial cells. *Digestion,* **77**, 108-117. doi:10.1159/000123840

**Beyenbach, K. W. and Piermarini, P. M.** (2011). Transcellular and paracellular pathways of transepithelial fluid secretion in Malpighian (renal) tubules of the yellow fever mosquito *Aedes aegypti*. *Acta Physiol.* **202**, 387-407. doi:10.1111/j.1748-1716.2010.02195.x

**Beyenbach, K. W., Baumgart, S., Lau, K., Piermarini, P. M. and Zhang, S.** (2009). Signaling to the apical membrane and to the paracellular pathway: changes in the cytosolic proteome of *Aedes* Malpighian tubules. *J. Exp. Biol.* **212**, 329-340. doi:10.1242/jeb.024646

**Bleich, M. and Warth, R.** (2000). The very small-conductance $K^+$ channel KVLQT1 and epithelial function. *Pflügers Arch. Euro. J. Physiol.* **440**, 202-206.

**Bradley, T. J.** (1987). Physiology of osmoregulation in mosquitoes. *Annu Rev. Entomol.* **32**, 439-462. doi:10.1146/annurev.en.32.010187.002255

**Bradley, T. J.** (1994). The role of physiological capacity, morphology and phylogeny in determining habitat use in mosquitoes. In *Ecological Morphology: Integrative Organismal Biology* (ed. P. C. Wainwright and S. M. Reilly), pp. 303-318. Chicago, IL: University of Chicago Press.

**Brennan, S. A., Grob, I. C., Bartz, C. E., Baker, J. K. and Jiang, Y.** (2021). Displacement of *Aedes albopictus* by *Aedes aegypti* in Gainesville, Florida. *J. Am. Mosq. Control Assoc.* **37**, 93-97. doi:10.2987/20-6992.1

**Calkins, T. and Piermarini, P.** (2017). A blood meal enhances innexin mRNA expression in the midgut, malpighian tubules, and ovaries of the yellow fever mosquito *Aedes aegypti*. *Insects* **8**, 122. doi:10.3390/insects8040122

**Cao-Pham, A. H., Hiong, K. C., Boo, M. V., Choo, C. Y. L., Wong, W. P., Chew, S. F. and Ip, Y. K.** (2019). Calcium absorption in the fluted giant clam, *Tridacna squamosa*, may involve a homolog of voltage-gated calcium channel subunit α1 (CACNA1) that has an apical localization and displays light-enhanced protein expression in the ctenidium. *J. Comp. Physiol. B* **189**, 693-706. doi:10.1007/s00360-019-01238-4

**Catterall, W. A.** (2011). Voltage-gated calcium channels. *Cold Spring Harb. Perspect. Biol.* **3**, a003947. doi:10.1101/cshperspect.a003947

**Cheng, W. and Zheng, J.** (2021). Distribution and assembly of TRP ion channels. *Adv. Exp. Med. Biol.* **1349**, 111-138. doi:10.1007/978-981-16-4254-8_7

**Coast, G. M.** (1998). The influence of neuropeptides on Malpighian tubule writhing and its significance for excretion. *Peptides* **19**, 469-480. doi:10.1016/S0196-9781(97)00461-0

**Corfas, R. A. and Vosshall, L. B.** (2015). The cation channel TRPA1 tunes mosquito thermotaxis to host temperatures. *Elife* **4**, e11750. doi:10.7554/eLife.11750

**de Brito Arduino, M., Mucci, L. F., Serpa, L. L. N. and de Rodrigues, M. M.** (2015). Effect of salinity on the behavior of *Aedes aegypti* populations from the coast and plateau of southeastern Brazil. *J. Vector Borne Dis.* **52**, 79-87.

**Del Duca, O., Nasirian, A., Galperin, V. and Donini, A.** (2011). Pharmacological characterisation of apical $Na^+$ and $Cl^-$ transport mechanisms of the anal papillae in the larval mosquito *Aedes aegypti*. *J. Exp. Biol.* **214**, 3992-3999. doi:10.1242/jeb.063719

**Demolombe, S., Franco, D., de Boer, P., Kuperschmidt, S., Roden, D., Pereon, Y., Jarry, A., Moorman, A. F. M. and Escande, D.** (2001). Differential expression of KvLQT1 and its regulator IsK in mouse epithelia. *Am. J. Physiol. Cell Physiol.* **280**, C359-C372. doi:10.1152/ajpcell.2001.280.2.C359

**Donini, A. and O'Donnell, M. J.** (2005). Analysis of $Na^+$, $Cl^-$, $K^+$, $H^+$ and $NH_4^+$ concentration gradients adjacent to the surface of anal papillae of the mosquito *Aedes aegypti*: application of self-referencing ion-selective microelectrodes. *J. Exp. Biol.* **208**, 603-610. doi:10.1242/jeb.01422

**Donini, A., Patrick, M. L., Bijelic, G., Christensen, R. J., Ianowski, J. P., Rheault, M. R. and O'Donnell, M. J.** (2006). Secretion of water and ions by Malpighian tubules of larval mosquitoes: effects of diuretic factors, second messengers, and salinity. *Physiol. Biochem. Zool.* **79**, 645-655. doi:10.1086/501059

**Donini, A., Gaidhu, M. P., Strasberg, D. R. and O'Donnell, M. J.** (2007). Changing salinity induces alterations in hemolymph ion concentrations and $Na^+$ and $Cl^-$ transport kinetics of the anal papillae in the larval mosquito, *Aedes aegypti*. *J. Exp. Biol.* **210**, 983-992. doi:10.1242/jeb.02732

**Donnelly, M. A. P., Kluh, S., Snyder, R. E. and Barker, C. M.** (2020). Quantifying sociodemographic heterogeneities in the distribution of *Aedes aegypti* among California households. *PLoS Negl. Trop. Dis.* **14**, e0008408. doi:10.1371/journal.pntd.0008408

**Drake, L. L., Boudko, D. Y., Marinotti, O., Carpenter, V. K., Dawe, A. L. and Hansen, I. A.** (2010). The Aquaporin gene family of the yellow fever mosquito, *Aedes aegypti*. *PLoS One* **5**, e15578. doi:10.1371/journal.pone.0015578

**Duong, P. C., McCabe, T. C., Riley, G. F., Holmes, H. L., Piermarini, P. M., Romero, M. F. and Gillen, C. M.** (2022). Sequence analysis and function of mosquito aeCCC2 and *Drosophila* Ncc83 orthologs. *Insect Biochem. Mol. Biol.* **143**, 103729. doi:10.1016/j.ibmb.2022.103729

**Durant, A. C., Guardian, E. G., Kolosov, D. and Donini, A.** (2021). The transcriptome of anal papillae of Aedes aegypti reveals their importance in xenobiotic detoxification and adds significant knowledge on ion, water and ammonia transport mechanisms. *J. Insect Physiol.* **132**, 104269. doi:10.1016/j.jinsphys.2021.104269

**Edwards, H. A.** (1982). Ion concentration and activity in the haemolymph of *Aedes aegypti* larvae. *J. Exp. Biol.* **101**, 143-151. doi:10.1242/jeb.101.1.143

**Edwards, H. A.** (1983). Electrophysiology of mosquito anal papillae. *J. Exp. Biol.* **102**, 343-346. doi:10.1242/jeb.102.1.343

**Edwards, H. A. and Harrison, J. B.** (1983). An osmoregulatory syncytium and associated cells in a freshwater mosquito. *Tissue Cell* **15**, 271-280. doi:10.1016/0040-8166(83)90022-8

**Efetova, M., Petereit, L., Rosiewicz, K., Overend, G., Haußig, F., Hovemann, B. T., Cabrero, P., Dow, J. A. and Schwärzel, M.** (2013). Separate roles of PKA and EPAC in renal function unraveled by the optogenetic control of cAMP levels in vivo. *J. Cell. Sci.* **126**, 778-788. doi:10.1242/jcs.114140

**Esquivel, C. J., Cassone, B. J. and Piermarini, P. M.** (2014). Transcriptomic evidence for a dramatic functional transition of the malpighian tubules after a blood meal in the Asian tiger mosquito *Aedes albopictus*. *PLoS Negl. Trop. Dis.* **8**, e2929. doi:10.1371/journal.pntd.0002929

**Esquivel, C. J., Cassone, B. J. and Piermarini, P. M.** (2016). A de novo transcriptome of the Malpighian tubules in non-blood-fed and blood-fed Asian tiger mosquitoes *Aedes albopictus*: insights into diuresis, detoxification, and blood meal processing. *PeerJ* **4**, e1784. doi:10.7717/peerj.1784

**Gioino, P., Murray, B. G. and Ianowski, J. P.** (2014). Serotonin triggers cAMP and PKA-mediated intracellular calcium waves in Malpighian tubules of *Rhodnius prolixus*. *Am. J. Physiol. Regul. Integr. Comp. Physiol.* **307**, R828-R836. doi:10.1152/ajpregu.00561.2013

**Giordano, B. V., Gasparotto, A., Liang, P., Nelder, M. P., Ru, C. and Hunter, F. F.** (2020). Discovery of an *Aedes* (Stegomyia) *albopictus* population and first records of *Aedes* (*Stegomyia*) *aegypti* in Canada. *Med. Vet. Entomol.* **34**, 10-16. doi:10.1111/mve.12408

**Goecks, J., Nekrutenko, A. and Taylor, J. and Galaxy Team, T.** (2010). Galaxy: a comprehensive approach for supporting accessible, reproducible, and transparent computational research in the life sciences. *Genome Biol.* **11**, R86. doi:10.1186/gb-2010-11-8-r86

**Gong, J., Nirala, N. K., Chen, J., Wang, F., Gu, P., Wen, Q., Ip, Y. T. and Xiang, Y.** (2023). TrpA1 is a shear stress mechanosensing channel regulating intestinal stem cell proliferation in *Drosophila*. *Sci. Adv.* **9**, eadc9660. doi:10.1126/sciadv.adc9660

**Inocente, E. A., Shaya, M., Acosta, N., Rakotondraibe, L. H. and Piermarini, P. M.** (2018). A natural agonist of mosquito TRPA1 from the medicinal plant *Cinnamosma fragrans* that is toxic, antifeedant, and repellent to the yellow fever

mosquito *Aedes aegypti*. *PLoS Negl. Trop. Dis.* **12**, e0006265. doi:10.1371/journal.pntd.0006265

**Ionescu, A. and Donini, A.** (2012). AedesCAPA-PVK-1 displays diuretic and dose dependent antidiuretic potential in the larval mosquito *Aedes aegypti* (Liverpool). *J. Insect Physiol.* **58**, 1299-1306. doi:10.1016/j.jinsphys.2012.07.002

**Jonusaite, S., Kelly, S. P. and Donini, A.** (2016). The response of claudin-like transmembrane septate junction proteins to altered environmental ion levels in the larval mosquito *Aedes aegypti*. *J. Comp. Physiol. B* **186**, 589-602. doi:10.1007/s00360-016-0979-z

**Jonusaite, S., Donini, A. and Kelly, S. P.** (2017). Salinity alters snakeskin and mesh transcript abundance and permeability in midgut and Malpighian tubules of larval mosquito, *Aedes aegypti*. *Comp. Biochem. Physiol. A* **205**, 58-67. doi:10.1016/j.cbpa.2016.12.015

**Kapoor, D., Khan, A., O'Donnell, M. J. and Kolosov, D.** (2021). Novel mechanisms of epithelial ion transport: insights from the cryptonephridial system of lepidopteran larvae. *Curr. Opin. Insect Sci.* **47**, 53-61. doi:10.1016/j.cois.2021.04.001

**Kariev, A. M. and Green, M. E.** (2012). Voltage gated ion channel function: gating, conduction, and the role of water and protons. *Intern. J. Mol. Sci.* **13**, 1680-1709. doi:10.3390/ijms13021680

**Khan, S. U., Ogden, N. H., Fazil, A. A., Gachon, P. H., Dueymes, G. U., Greer, A. L. and Ng, V.** (2020). Current and projected distributions of *Aedes aegypti* and *Ae. albopictus* in Canada and the U.S. *Environ. Health Perspect.* **128**, 57007. doi:10.1289/EHP5899

**Kho, M., Smith, J. A., Verweij, N., Shang, L., Ryan, K. A., Zhao, W., Ware, E. B., Gansevoort, R. T., Irvin, M. R., Lee, J. E. et al.** (2020). Genome-wide association meta-analysis of individuals of European ancestry identifies suggestive loci for sodium intake, potassium intake, and their ratio measured from 24-h or half-day urine samples. *J. Nutr.* **150**, 2635-2645. doi:10.1093/jn/nxaa241

**Ko, H.-K., Lin, A.-H., Perng, D.-W., Lee, T.-S. and Kou, Y. R.** (2020). Lung epithelial TRPA1 mediates lipopolysaccharide-induced lung inflammation in bronchial epithelial cells and mice. *Front. Physiol.* **11**, 596314. doi:10.3389/fphys.2020.596314

**Koch, H. J.** (1938). The absorption of chloride ions by the anal papillae of Diptera larvae. *J. Exp. Biol.* **15**, 152-160. doi:10.1242/jeb.15.1.152

**Kolosov, D. and Kelly, S. P.** (2017). Claudin-8d is a cortisol-responsive barrier protein in the gill epithelium of trout. *J. Mol. Endocrinol.* **59**, 299-310. doi:10.1530/JME-17-0108

**Kolosov, D. and O'Donnell, M. J.** (2019). Malpighian tubules of caterpillars: blending RNAseq and physiology to reveal regional functional diversity and novel epithelial ion transport control mechanisms. *J. Exp. Biol.* **222**, jeb211623. doi:10.1242/jeb.211623

**Kolosov, D. and O'Donnell, M. J.** (2020). Mechanisms and regulation of chloride transport in the Malpighian tubules of the larval cabbage looper *Trichoplusia ni*. *Insect Biochem. Mol. Biol.* **116**, 103263. doi:10.1016/j.ibmb.2019.103263

**Kolosov, D. and O'Donnell, M. J.** (2022). Blending physiology and RNAseq to provide new insights into regulation of epithelial transport: switching between ion secretion and reabsorption. *J. Exp. Biol.* **225**, jeb243293. doi:10.1242/jeb.243293

**Kolosov, D., Tauqir, M., Rajaruban, S., Piermarini, P. M., Donini, A. and O'Donnell, M. J.** (2018a). Molecular mechanisms of bi-directional ion transport in the Malpighian tubules of a lepidopteran crop pest, *Trichoplusia ni*. *J. Insect Physiol.* **109**, 55-68. doi:10.1016/j.jinsphys.2018.06.005

**Kolosov, D., Piermarini, P. M. and O'Donnell, M. J.** (2018b). Malpighian tubules of *Trichoplusia ni*: recycling ions via gap junctions and switching between secretion and reabsorption of $Na^+$ and $K^+$ in the distal ileac plexus. *J. Exp. Biol.* **221**, jeb172296. doi:10.1242/jeb.172296

**Kolosov, D., Donly, C., MacMillan, H. and O'Donnell, M. J.** (2019). Transcriptomic analysis of the Malpighian tubules of *Trichoplusia ni*: clues to mechanisms for switching from ion secretion to ion reabsorption in the distal ileac plexus. *J. Insect Physiol.* **112**, 73-89. doi:10.1016/j.jinsphys.2018.12.005

**Kolosov, D., Leonard, E. M. and O'Donnell, M. J.** (2021). Voltage-gated calcium channels regulate $K^+$ transport in the Malpighian tubules of the larval cabbage looper, *Trichoplusia ni*. *J. Insect Physiol.* **131**, 104230. doi:10.1016/j.jinsphys.2021.104230

**Lai, K. P., Li, J.-W., Gu, J., Chan, T.-F., Tse, W. K. F. and Wong, C. K. C.** (2015). Transcriptomic analysis reveals specific osmoregulatory adaptive responses in gill mitochondria-rich cells and pavement cells of the Japanese eel. *BMC Genomics* **16**, 1072. doi:10.1186/s12864-015-2271-0

**Lee, Y., Lee, Y., Lee, J., Bang, S., Hyun, S., Kang, J., Hong, S.-T., Bae, E., Kaang, B.-K. and Kim, J.** (2005). Pyrexia is a new thermal transient receptor potential channel endowing tolerance to high temperatures in Drosophila melanogaster. *Nat. Genet.* **37**, 305-310. doi:10.1038/ng1513

**Lee, Y., Schmidt, H., Collier, T. C., Conner, W. R., Hanemaaijer, M. J., Slatkin, M., Marshall, J. M., Chiu, J. C., Smartt, C. T., Lanzaro, G. C. et al.** (2019). Genome-wide divergence among invasive populations of *Aedes aegypti* in California. *BMC Genomics* **20**, 204. doi:10.1186/s12864-019-5586-4

**Li, Y., Piermarini, P. M., Esquivel, C. J., Price, D. P., Drumm, H. E., Schilkey, F. D. and Hansen, I. A.** (2017). RNA-Seq comparison of larval and adult Malpighian tubules of the yellow fever mosquito aedes aegypti reveals life stage-specific changes in renal function. *Front. Physiol.* **8**, 283. doi:10.3389/fphys.2017.00283

**Lounibos, L. P. and Kramer, L. D.** (2016). Invasiveness of *Aedes aegypti* and *Aedes albopictus* and vectorial capacity for Chikungunya virus. *J. Infect. Dis.* **214**, S453-S458. doi:10.1093/infdis/jiw285

**Love, M. I., Huber, W. and Anders, S.** (2014). Moderated estimation of fold change and dispersion for RNA-seq data with DESeq2. *Genome Biol.* **15**, 550. doi:10.1186/s13059-014-0550-8

**Lozano, R., Naghavi, M., Foreman, K., Lim, S., Shibuya, K., Aboyans, V., Abraham, J., Adair, T., Aggarwal, R., Ahn, S. Y. et al.** (2012). Global and regional mortality from 235 causes of death for 20 age groups in 1990 and 2010: a systematic analysis for the Global Burden of Disease Study 2010. *Lancet* **380**, 2095-2128. doi:10.1016/S0140-6736(12)61728-0

**Mack, L. K., Kelly, E. T., Lee, Y., Brisco, K. K., Shen, K. V., Zahid, A., van Schoor, T., Cornel, A. J. and Attardo, G. M.** (2021). Frequency of sodium channel genotypes and association with pyrethrum knockdown time in populations of Californian *Aedes aegypti*. *Parasit. Vector.* **14**, 141. doi:10.1186/s13071-021-04627-3

**Mao, F., Lu, W.-J., Yang, Y., Qiao, X., Ye, G.-Y. and Huang, J.** (2020). Identification, characterization and expression analysis of TRP channel genes in the vegetable pest, *Pieris rapae*. *Insects* **11**, 192. doi:10.3390/insects11030192

**Marusalin, J., Matier, B. J., Rheault, M. R. and Donini, A.** (2012). Aquaporin homologs and water transport in the anal papillae of the larval mosquito, *Aedes aegypti*. *J. Comp. Physiol. B.* **182**, 1047-1056. doi:10.1007/s00360-012-0679-2

**McLaughlin, K. A. and Levin, M.** (2018). Bioelectric signaling in regeneration - mechanisms of ionic controls of growth and form. *Dev. Biol.* **433**, 177-189. doi:10.1016/j.ydbio.2017.08.032

**Misyura, L., Grieco Guardian, E., Durant, A. C. and Donini, A.** (2020). A comparison of aquaporin expression in mosquito larvae (*Aedes aegypti*) that develop in hypo-osmotic freshwater and iso-osmotic brackish water. *PloS One,* **15**, e0234892. doi:10.1371/journal.pone.0234892

**Mondejar-Parreño, G., Perez-Vizcaino, F. and Cogolludo, A.** (2020). Kv7 channels in lung diseases. *Frontier. Physiol.* **11**, 634. doi:10.3389/fphys.2020.00634

**Monteil, A., Guérineau, N. C., Gil-Nagel, A., Parra-Diaz, P., Lory, P. and Senatore, A.** (2023). New insights into the physiology and pathophysiology of the atypical sodium leak channel NALCN. *Physiol. Rev.* **104**, 399-472. doi:10.1152/physrev.00014.2022

**Morera, F. J., Saravia, J., Pontigo, J. P., Vargas-Chacoff, L., Contreras, G. F., Pupo, A., Lorenzo, Y., Castillo, K., Tilegenova, C., Cuello, L. G. et al.** (2015). Voltage-dependent BK and Hv1 channels expressed in non-excitable tissues: new therapeutics opportunities as targets in human diseases. *Pharmacol. Res.* **101**, 56-64. doi:10.1016/j.phrs.2015.08.011

**Nilius, B. and Droogmans, G.** (2001). Ion channels and their functional role in vascular endothelium. *Physiol. Rev.* **81**, 1415-1459. doi:10.1152/physrev.2001.81.4.1415

**Nilius, B., Appendino, G. and Owsianik, G.** (2012). The transient receptor potential channel TRPA1: from gene to pathophysiology. *Pflügers Arch. Eur. J. Physiol.* **464**, 425-458. doi:10.1007/s00424-012-1158-z

**Parker, C., Ramirez, D. and Connelly, C. R.** (2019). State-wide survey of *Aedes aegypti* and *Aedes albopictus* (Diptera: Culicidae) in Florida. *J. Vector Ecol.* **44**, 210-215. doi:10.1111/jvec.12351

**Patrick, M. L. and Bradley, T. J.** (2000). The physiology of salinity tolerance in larvae of two species of *Culex* mosquitoes: the role of compatible solutes. *J. Exp. Biol.* **203**, 821-830. doi:10.1242/jeb.203.4.821

**Patrick, M. L., Gonzalez, R. J. and Bradley, T. J.** (2001). Sodium and chloride regulation in freshwater and osmoconforming larvae of *Culex* mosquitoes. *J. Exp. Biol.* **204**, 3345-3354. doi:10.1242/jeb.204.19.3345

**Patrick, M. L., Aimanova, K., Sanders, H. R. and Gill, S. S.** (2006). P-type $Na^+/K^+$-ATPase and V-type $H^+$-ATPase expression patterns in the osmoregulatory organs of larval and adult mosquito Aedes aegypti. *J. Exp. Biol.* **209**, 4638-4651. doi:10.1242/jeb.02551

**Patro, R., Duggal, G., Love, M. I., Irizarry, R. A. and Kingsford, C.** (2017). Salmon provides fast and bias-aware quantification of transcript expression. *Nat. Methods* **14**, 417-419. doi:10.1038/nmeth.4197

**Piermarini, P. M. and Gillen, C. M.** (2015). Non-traditional models: the molecular physiology of sodium and water transport in mosquito Malpighian tubules. In *Sodium and Water Homeostasis* (ed. K. A. Hyndman and T. L. Pannabecker), pp. 255-278. New York, NY: Springer New York.

**Piermarini, P. M., Grogan, L. F., Lau, K., Wang, L. and Beyenbach, K. W.** (2010). A SLC4-like anion exchanger from renal tubules of the mosquito (*Aedes aegypti*): evidence for a novel role of stellate cells in diuretic fluid secretion. *Am. J. Physiol. Regul. Integr. Comp. Physiol.* **298**, R642-R660. doi:10.1152/ajpregu.00729.2009

**Piermarini, P., Esquivel, C. and Denton, J.** (2017a). Malpighian tubules as novel targets for mosquito control. *Int. J. Environ. Res. Public Health* **14**, 111. doi:10.3390/ijerph14020111

**Piermarini, P. M., Akuma, D. C., Crow, J. C., Jamil, T. L., Kerkhoff, W. G., Viel, K. C. M. F. and Gillen, C. M.** (2017b). Differential expression of putative sodium-dependent cation-chloride cotransporters in *Aedes aegypti*. *Comp. Biochem. Physiol. A* **214**, 40-49. doi:10.1016/j.cbpa.2017.09.007

**Pitt, G. S., Matsui, M. and Cao, C.** (2021). Voltage-gated calcium channels in nonexcitable tissues. *Ann. Rev. Physiol.* **83**, 183-203. doi:10.1146/annurev-physiol-031620-091043

**Preston, P., Wartosch, L., Günzel, D., Fromm, M., Kongsuphol, P., Ousingsawat, J., Kunzelmann, K., Barhanin, J., Warth, R. and Jentsch, T. J.** (2010). Disruption of the $K^+$ channel β-Subunit KCNE3 reveals an important role in intestinal and tracheal $Cl^-$ transport. *J. Biol. Chem.* **285**, 7165-7175. doi:10.1074/jbc.M109.047829

**Ramasamy, R. and Surendran, S. N.** (2012). Global climate change and its potential impact on disease transmission by salinity-tolerant mosquito vectors in coastal zones. *Front Physiol.* **3**, 198. doi:10.3389/fphys.2012.00198

**Ramasamy, R. and Surendran, S. N.** (2016). Mosquito vectors developing in atypical anthropogenic habitats: global overview of recent observations, mechanisms and impact on disease transmission. *J. Vector Borne Dis.* **53**, 91-98.

**Ramasamy, R., Surendran, S. N., Jude, P. J., Dharshini, S. and Vinobaba, M.** (2011). Larval development of *Aedes aegypti* and *Aedes albopictus* in peri-urban brackish water and its implications for transmission of arboviral diseases. *PLoS Negl. Trop. Dis.* **5**, e1369. doi:10.1371/journal.pntd.0001369

**Ramasamy, R., Jude, P. J., Veluppillai, T., Eswaramohan, T. and Surendran, S. N.** (2014). Biological differences between brackish and fresh water-derived *Aedes aegypti* from two locations in the Jaffna peninsula of Sri Lanka and the implications for arboviral disease transmission. *PLoS One* **9**, e104977. doi:10.1371/journal.pone.0104977

**Ramasamy, R., Thiruchenthooran, V., Jayadas, T. T. P., Eswaramohan, T., Santhirasegaram, S., Sivabalakrishnan, K., Naguleswaran, A., Uzest, M., Cayrol, B., Voisin, S. N. et al.** (2021). Transcriptomic, proteomic and ultrastructural studies on salinity-tolerant *Aedes aegypti* in the context of rising sea levels and arboviral disease epidemiology. *BMC Genom.* **22**, 253. doi:10.1186/s12864-021-07564-8

**Ramsay, J. A.** (1953). Exchanges of sodium and potassium in mosquito larvae. *J. Exp. Biol.* **30**, 79-89. doi:10.1242/jeb.30.1.79

**Rasmussen, R. N., Christensen, K. V., Holm, R. and Nielsen, C. U.** (2019). Transcriptome analysis identifies activated signaling pathways and regulated ABC transporters and solute carriers after hyperosmotic stress in renal MDCK I cells. *Genomics* **111**, 1557-1565. doi:10.1016/j.ygeno.2018.10.014

**Robert, C. and Watson, M.** (2015). Errors in RNA-Seq quantification affect genes of relevance to human disease. *Genome Biol.* **16**, 177. doi:10.1186/s13059-015-0734-x

**Sajadi, F., Curcuruto, C., Al Dhaheri, A. and Paluzzi, J.-P. V.** (2018). Anti-diuretic action of a CAPA neuropeptide against a subset of diuretic hormones in the disease vector *Aedes aegypti*. *J. Exp. Biol.* **221**, jeb177089. doi:10.1242/jeb.177089

**Salgado, V. L.** (2017). Insect TRP channels as targets for insecticides and repellents. *J. Pesticide Sci.* **42**, 1-6. doi:10.1584/jpestics.D16-104

**Scheffers, B. R., De Meester, L., Bridge, T. C. L., Hoffmann, A. A., Pandolfi, J. M., Corlett, R. T., Butchart, S. H. M., Pearce-Kelly, P., Kovacs, K. M., Dudgeon, D. et al.** (2016). The broad footprint of climate change from genes to biomes to people. *Science* **354**, aaf7671. doi:10.1126/science.aaf7671

**Schönherr, R., Löber, K. and Heinemann, S. H.** (2000). Inhibition of human ether à go-go potassium channels by $Ca^{2+}$/calmodulin. *EMBO J.* **19**, 3263-3271. doi:10.1093/emboj/19.13.3263

**Schroeder, B. C., Waldegger, S., Fehr, S., Bleich, M., Warth, R., Greger, R. and Jentsch, T. J.** (2000). A constitutively open potassium channel formed by KCNQ1 and KCNE3. *Nature* **403**, 196-199. doi:10.1038/35003200

**Shi, W. M., Wymore, R. S., Wang, H. S., Pan, Z. M., Cohen, I. S., McKinnon, D. and Dixon, J. E.** (1997). Identification of two nervous system-specific members of the erg potassium channel gene family. *J. Neurosci.* **17**, 9423-9432. doi:10.1523/JNEUROSCI.17-24-09423.1997

**Sillanpää, J. K., Cardoso, J. C. D. R., Félix, R. C., Anjos, L., Power, D. M. and Sundell, K.** (2020). Dilution of Seawater Affects the $Ca^{2+}$ Transport in the Outer Mantle Epithelium of *Crassostrea gigas*. *Front. Physiol,* **11**, 1. doi:10.3389/fphys.2020.00001

**Sinke, A. P., Caputo, C., Tsaih, S.-W., Yuan, R., Ren, D., Deen, P. M. T. and Korstanje, R.** (2011). Genetic analysis of mouse strains with variable serum sodium concentrations identifies the Nalcn sodium channel as a novel player in osmoregulation. *Physiol. Genomics.* **43**, 265-270. doi:10.1152/physiolgenomics.00188.2010

**Siroky, B. J., Kleene, N. K., Kleene, S. J., Varnell, C. D., Jr, Comer, R. G., Liu, J., Lu, L., Pachciarz, N. W., Bissler, J. J. and Dixon, B. P.** (2017). Primary cilia regulate the osmotic stress response of renal epithelial cells through TRPM3. *Am. J. Physiol. Renal Physiol.* **312**, F791-F805. doi:10.1152/ajprenal.00465.2015

**Sohal, R. S. and Copeland, E.** (1966). Ultrastructural variations in the anal papillae of *Aedes aegypti* (L) at different environmental salinities. *J. Insect Physiol.* **12**, 429-434. doi:10.1016/0022-1910(66)90006-0

**Stobbart, R. H.** (1971). The control of sodium uptake by the larva of the mosquito *Aedes aegypti* (L.). *J. Exp. Biol.* **54**, 29-66. doi:10.1242/jeb.54.1.29

**Su, H.-A., Bai, X., Zeng, T., Lu, Y.-Y. and Qi, Y.-X.** (2018). Identification, characterization and expression analysis of transient receptor potential channel genes in the oriental fruit fly, *Bactrocera dorsalis*. *BMC Genomics* **19**, 674. doi:10.1186/s12864-018-5053-7

**Surendran, S. N., Jude, P. J., Thabothiny, V., Raveendran, S. and Ramasamy, R.** (2012). Pre-imaginal development of *Aedes aegypti* in brackish and fresh water urban domestic wells in Sri Lanka. *J. Vector Ecol.* **37**, 471-473. doi:10.1111/j.1948-7134.2012.00254.x

**Surendran, S. N., Sivabalakrishnan, K., Jayadas, T. T. P., Santhirasegaram, S., Laheetharan, A., Senthilnanthanan, M. and Ramasamy, R.** (2018a). Adaptation of *Aedes aegypti* to salinity: characterized by larger anal papillae in larvae. *J. Vector Borne Dis.* **55**, 235-238. doi:10.4103/0972-9062.249482

**Surendran, S. N., Veluppillai, T. and Eswaramohan, T., Sivabalakrishnan, K., Noordeen, F. and Ramasamy, R.** (2018b). Salinity tolerant *Aedes aegypti* and *Ae. albopictus*—infection with dengue virus and contribution to dengue transmission in a coastal peninsula. *J. Vector Borne Dis.* **55**, 26-33. doi:10.4103/0972-9062.234623

**Swayne, L. A., Mezghrani, A., Lory, P., Nargeot, J. and Monteil, A.** (2010). The NALCN ion channel is a new actor in pancreatic β-cell physiology. *Islets* **2**, 54-56. doi:10.4161/isl.2.1.10522

**Talavera, K., Startek, J. B., Alvarez-Collazo, J., Boonen, B., Alpizar, Y. A., Sanchez, A., Naert, R. and Nilius, B.** (2020). Mammalian transient receptor potential TRPA1 channels: from structure to disease. *Physiol. Rev.* **100**, 725-803. doi:10.1152/physrev.00005.2019

**Tiburcy, F., Beyenbach, K. W. and Wieczorek, H.** (2013). Protein kinase A-dependent and -independent activation of the V-ATPase in Malpighian tubules of *Aedes aegypti*. *J. Exp. Biol.* **216**, 881-891. doi:10.1242/jeb.078360

**Tracey, W. D., Wilson, R. I., Laurent, G. and Benzer, S.** (2003). Painless, a Drosophila gene essential for nociception. *Cell* **113**, 261-273. doi:10.1016/S0092-8674(03)00272-1

**Treherne, J. E.** (1954). The exchange of labelled sodium in the larva of *Aedes aegypti* L. *J. Exp. Biol.* **31**, 386-401. doi:10.1242/jeb.31.3.386

**van der Horst, J., Greenwood, I. A. and Jepps, T. A.** (2020). Cyclic AMP-dependent regulation of Kv7 voltage-gated potassium channels. *Front. Physiol.* **11**, 727. doi:10.3389/fphys.2020.00727

**Van Liefferinge, E., Van Noten, N., Degroote, J., Vrolix, G., Van Poucke, M., Peelman, L., Van Ginneken, C., Roura, E. and Michiels, J.** (2020). Expression of transient receptor potential ankyrin 1 and transient receptor potential vanilloid 1 in the gut of the peri-weaning pig is strongly dependent on age and intestinal site. *Animals* **10**, 2417. doi:10.3390/ani10122417

**Vanneste, M., Segal, A., Voets, T. and Everaerts, W.** (2021). Transient receptor potential channels in sensory mechanisms of the lower urinary tract. *Nat. Rev. Urol.* **18**, 139-159. doi:10.1038/s41585-021-00428-6

**Venkatachalam, K. and Montell, C.** (2007). TRP channels. *Ann. Rev. Biochem.* **76**, 387-417. doi:10.1146/annurev.biochem.75.103004.142819

**Wahl-Schott, C. and Biel, M.** (2009). HCN channels: structure, cellular regulation and physiological function. *Cell. Mol. Life Sci.* **66**, 470-494. doi:10.1007/s00018-008-8525-0

**Warmke, J. W., Reenan, R. A., Wang, P., Qian, S., Arena, J. P., Wang, J., Wunderler, D., Liu, K., Kaczorowski, G. J., Ploeg, L. H. T. V. et al.** (1997). Functional expression of *Drosophila* para sodium channels. Modulation by the membrane protein TipE and toxin pharmacology. *J. Gen. Physiol.* **110**, 119-133. doi:10.1085/jgp.110.2.119

**Weng, X. H., Piermarini, P. M., Yamahiro, A., Yu, M. J., Aneshansley, D. J. and Beyenbach, K. W.** (2008). Gap junctions in Malpighian tubules of Aedes aegypti. *J. Exp. Biol.* **211**, 409-422. doi:10.1242/jeb.011213

**Wigglesworth, V. B.** (1933). The adaptation of mosquito larvae to salt water. *J. Exp. Biol.* **10**, 27-36. doi:10.1242/jeb.10.1.27

**World Health Organization** (2014). *A global brief on vector-borne diseases*. World Health Organization. https://apps.who.int/iris/handle/10665/111008

**Xie, J., Ke, M., Xu, L., Lin, S., Huang, J., Zhang, J., Yang, F., Wu, J. and Yan, Z.** (2020). Structure of the human sodium leak channel NALCN in complex with FAM155A. *Nat. Commun.* **11**, 5831. doi:10.1038/s41467-020-19667-z

**Yang, H. and Cui, J.** (2015). BK channels. In *Handbook of Ion Channels* (ed. J. Zheng and M. C. Trudeau), pp. 247-260. CRC Press.

**Yu, M.-J. and Beyenbach, K. W.** (2002). Leucokinin activates $Ca^{2+}$-dependent signal pathway in principal cells of *Aedes aegypti* Malpighian tubules. *Am. J. Physiol. Renal. Physiol.* **283**, F499-F508. doi:10.1152/ajprenal.00041.2002

**Yuan, Y.-Y., Li, M., Fan, F. and Qiu, X.-H.** (2018). Comparative transcriptomic analysis of larval and adult Malpighian tubules from the cotton bollworm *Helicoverpa armigera*. *Insect Sci.* **25**, 991-1005. doi:10.1111/1744-7917.12561

**Yue, L. and Xu, H.** (2021). TRP channels in health and disease at a glance. *J. Cell Sci.* **134**, jcs258372. doi:10.1242/jcs.258372

**Zhu, M. X., Evans, M. D., Ma, J., Parrington, J. and Galione, A.** (2010). Two-pore channels for integrative $Ca^{2+}$ signaling. *Commun. Integr. Biol.* **3**, 12-17. doi:10.4161/cib.3.1.9793